Atmos. Chem. Phys., 25, 1227–1252, 2025
https://doi.org/10.5194/acp-25-1227-2025

Atmospheric Chemistry and Physics
Open Access
EGU

Long-term changes in the thermodynamic structure of the lowermost stratosphere inferred from reanalysis data

Franziska Weyland[1], Peter Hoor[1], Daniel Kunkel[1], Thomas Birner[2,3], Felix Plöger[4,5], and Katharina Turhal[4,5]

[1]Institute for Atmospheric Physics, Johannes Gutenberg University Mainz, Mainz, Germany
[2]Meteorological Institute, Ludwig-Maximilians-Universität München, Munich, Germany
[3]Institute for Physics of the Atmosphere, Deutsches Zentrum für Luft- und Raumfahrt, Oberpfaffenhofen, Germany
[4]Institute of Climate and Energy Systems, Stratosphere (ICE-4), Forschungszentrum Jülich, Jülich, Germany
[5]Institute for Atmospheric and Environmental Research, University of Wuppertal, Wuppertal, Germany

Correspondence: Franziska Weyland (franziska.weyland@uni-mainz.de)

Received: 5 June 2024 – Discussion started: 13 June 2024
Revised: 11 November 2024 – Accepted: 13 November 2024 – Published: 29 January 2025

Abstract. The lowermost stratosphere (LMS) plays an important role in stratosphere–troposphere coupling and the Earth's radiation balance. This study investigates the effects of long-term changes in the tropopause and the lower-stratospheric isentropic structure on the mass of the LMS. We compare five modern reanalyses: ERA5, ERA-Interim, MERRA-2, JRA-55 and JRA-3Q. The focus is on changes after 1998, which marks the anticipated beginning of stratospheric ozone recovery. The trend analysis is performed with a dynamic linear regression model (DLM), capable of modeling non-linear trends. According to our study, isentropic pressure in the lower stratosphere (here 380–430 K) shows negative trends in the tropics and positive trends in the extratropics. In the Northern Hemisphere (NH), we find that the extratropical tropopause is rising, accompanied by decreasing pressure at an average rate of −1 hPa per decade. Additionally, our results indicate that the tropical tropopause in the NH has expanded poleward by 0.5° latitude between 1998–2019. In the Southern Hemisphere (SH) extratropics, the lapse rate tropopause shows a downward tendency of up to +2 hPa per decade after 1998, consistent across all reanalyses except JRA-3Q. The tropical tropopause and the cold point is rising, accompanied by decreasing pressure at a rate of ca. −0.5 hPa per decade in all reanalyses. The sign of the tropical tropopause potential temperature trends, however, differs across the reanalyses. This can be attributed to contrasting (absolute) temperature trends in the tropical tropopause region, such as at the 100 hPa pressure level. Consistent with the upward and poleward trend of the NH tropopause, the mass of the LMS decreases by 2 %–3 % for 1998–2019 if a fixed isentrope (380 K) is chosen as the upper LMS boundary. In ERA5, as well as MERRA-2 and ERA-Interim, this mass decline disappears if dynamical upper LMS boundaries are used that take the upward trends of the tropical tropopause into account.

1 Introduction

The lowermost stratosphere (LMS), also referred to as the stratospheric part of the "middle world", is defined as the region of the stratosphere where isentropic surfaces intersect with the tropopause (Holton et al., 1995). The middle world can be distinguished from the "overworld", where isentropes are situated entirely in the stratosphere, and the "underworld", with isentropes exclusively located in the troposphere (Hoskins, 1991). Along these intersecting isentropes, quasi-isentropic exchange between the tropical troposphere and the extratropical stratosphere is possible. The upper boundary of the LMS has often been approximated by the 380 K isentrope, which, in turn, can be regarded as an approximation of the trop-

ical tropopause (e.g., Appenzeller et al., 1996; Schoeberl, 2004; Olsen et al., 2013; Wang and Fu, 2021). The LMS includes the extratropical transition layer (ExTL) (WMO, 2003), which has been defined on the basis of trace gas gradient changes in the LMS (e.g., Hoor et al., 2004), consistent with trajectory studies (Berthet et al., 2007). The ExTL is characterized by irreversible mixing across the tropopause and high variability of radiatively relevant trace gases like water vapor and ozone (Pan et al., 2004; Hoor et al., 2002; Fischer et al., 2000). The ExTL partly coincides with the tropopause inversion layer (TIL) as marked by a maximum of static stability (Birner et al., 2002; Birner, 2006). Further, the ExTL region is characterized by strong shear occurrence just around the extratropical tropopause (Kunkel et al., 2019; Kaluza et al., 2021). The LMS is essential for the Earth's radiation budget (e.g., Forster and Shine, 1997, 2002; Zhang et al., 2004; Riese et al., 2012) since it constitutes a region of strong composition gradients of, e.g., ozone and water vapor. Changes in the LMS composition affect local temperature gradients (e.g., Randel et al., 2007) with impacts on climate and circulation (e.g., Hegglin and Shepherd, 2009; Charlesworth et al., 2023). Furthermore, the LMS contains a significant proportion of stratospheric mass, and thereby a considerable part of total column ozone, due to the exponential density decrease with altitude. From Fig. 5 in Appenzeller et al. (1996), the LMS mass can be estimated to be about 30 %–50 % of the total stratospheric mass. LMS and stratospheric mass shows a seasonal cycle, closely following the seasonal cycle of tropopause height (Appenzeller et al., 1996). On short timescales, LMS mass variations are linked to stratospheric–tropospheric mass exchange (e.g., Stohl, 2003; Schoeberl, 2004; Hegglin et al., 2010; Škerlak et al., 2014). This affects the abundance of trace gases such as ozone, which show sharp gradients in the upper troposphere–lower stratosphere (UTLS). Due to this transport barrier property, which gives rise to strong trace gas gradients, the tropopause location is of special importance.

The LMS is bounded below by the extratropical tropopause. The location of the (extratropical) tropopause can be defined thermally based on the temperature lapse rate (WMO, 1957) or the potential temperature gradient (Tinney et al., 2022), dynamically by choosing a characteristic value of potential vorticity (PV) (e.g., Hoerling et al., 1991) or by PV gradients (Kunz et al., 2011), and chemically via trace gas gradients (e.g., ozone) or trace gas correlations (e.g., Bethan et al., 1996; Fischer et al., 2000). The tropical tropopause level, which may serve as an upper boundary for the LMS, can be defined thermally by the (potential) temperature lapse rate or the cold point, i.e., the local temperature minimum (Holton et al., 1995), or as an isentrope, e.g., the potential temperature level of 380 K.

Since the tropopause is strongly coupled to the temperature profile in the lower and middle atmosphere, the tropopause height is sensitive to climate changes and variability. Specifically, the tropopause height has been shown to be a robust fingerprint of anthropogenic climate change. Increasing concentrations of well-mixed greenhouse gases (GHGs) lead to a warming of the troposphere and cooling of the stratosphere, reinforced by the depletion of stratospheric ozone. Warming of the troposphere and cooling of the stratosphere result in a tropopause rise (e.g., Seidel et al., 2001; Santer et al., 2004; Seidel and Randel, 2006). In addition to radiative effects, stratospheric dynamics, as manifested by the Brewer–Dobson circulation (BDC), affect the location of the tropopause and the Equator-to-pole contrast in tropopause height (Birner, 2010b).

A rise in the global tropopause of the order of 50–100 m per decade has been reported in many studies of radiosonde (e.g., Seidel and Randel, 2006; Xian and Homeyer, 2019; Meng et al., 2021) and satellite (e.g., Schmidt et al., 2008; Meng et al., 2021) observations as well as in reanalysis data (e.g., Wilcox et al., 2012; Xian and Homeyer, 2019) and climate models (e.g., Santer, 2003a) and for different tropopause definitions. Even though pressure surfaces are rising together with the tropopause as a result of the thermal expansion of the troposphere (e.g., Eichinger and Šácha, 2020), it has been found that tropopause pressure trends are negative of the order of −1 hPa per decade, apparently exceeding isobaric height trends (e.g., Santer, 2003a; Seidel and Randel, 2006; Wilcox et al., 2012). Natural variability has been found to play a minor role in tropopause trends (Sausen and Santer, 2003; Meng et al., 2021). Instead, model experiments by Santer (2003b) suggest that 80 % of the tropopause rise between 1979–1999 is attributable to anthropogenic influence, primarily increasing greenhouse gas emissions, and the resulting warming of the troposphere and cooling of the stratosphere. The tropospheric warming was found to cause a persistent lifting of the tropopause, even as contrasting temperature effects are expected in the stratosphere, where ozone recovery is causing warming, while increasing GHG load is exerting a cooling influence (Pisoft et al., 2021; Meng et al., 2021). In the tropics, the cold point is rising together with the lapse rate tropopause (e.g., Tegtmeier et al., 2020; Zou et al., 2023). Temperature trends in the tropical lower stratosphere and the cold point show large uncertainties. Tegtmeier et al. (2020) report small negative cold-point temperature trends for the time period 1979–2005 for different reanalyses. Results by Zou et al. (2023) agree for the same time period but suggest a warming of the tropical tropopause from 2006–2021 in ERA5. A similar trend behavior has been reported by Fu et al. (2019) for tropical tropopause layer (TTL) temperatures from satellite observations. Before 2000, temperatures show small but significant negative trends, consistent with Tegtmeier et al. (2020), but no trend thereafter.

The largest trends in tropopause height are usually apparent in the subtropics around the tropopause break, which can be associated with a transition from lower extratropical values to significantly higher levels characteristic of the tropical tropopause. This effect can be understood as

a broadening of the tropics and has been observed in radiosonde and satellite data (e.g., Seidel and Randel, 2007; Meng et al., 2021) as well as reanalysis data (e.g., Lu et al., 2009; Birner, 2010a; Wilcox et al., 2012). However, evidence of recent tropical narrowing has been reported by Zou et al. (2023). Xian and Homeyer (2019) find a dipole structure with regions of increasing and decreasing tropopause altitude around the mean tropopause break in different zonally resolved reanalyses for the time period 1981–2015. In latitude coordinates relative to the tropopause break, the dipole structure mostly disappears, and tropopause trends become the largest around the mean tropopause break, which agrees with zonal mean analyses. Robust tropical widening has also been documented based on other metrics that do not however necessarily correlate well with variations in the location of the tropopause break (e.g., Staten et al., 2018; Grise et al., 2019). Turhal et al. (2024) report a tropical widening above 370 K and below 340 K but a narrowing of the tropospheric width in the region in between for the isentropic PV-gradient tropopause from reanalysis data between 1980–2017. In addition to the general widening of the tropics, the frequency of double tropopause events, i.e., poleward excursions of the tropical tropopause above the extratropical tropopause, is found to have increased (Castanheira et al., 2009; Xian and Homeyer, 2019). This trend likely reflects an increase in baroclinicity in the UTLS, driven by GHG-induced climate change (Castanheira et al., 2009).

In addition to the observed long-term changes in the tropopause location, climate model projections agree on an acceleration of the Brewer–Dobson circulation (BDC) as a consequence of GHG-induced climate change (e.g., Butchart, 2014). According to Oberländer-Hayn et al. (2016) and Šácha et al. (2024), it is more precise to refer to a lifting of the circulation, which is connected to the tropopause expansion itself. Stratospheric temperature changes linked to stratospheric ozone additionally influence the BDC evolution. In response to the increased tropical upwelling (extratropical downwelling), resulting in adiabatic cooling (heating), the temperature structure of the stratosphere is expected to change.

Observations of the BDC behavior are only possible indirectly, and the different approaches give a less clear picture of recent BDC trends than model simulations. For example, Thompson and Solomon (2009) report trends of lower stratospheric temperature and ozone between 1979–2006 from satellite observations that agree with an increased BDC, consistent with findings by Tegtmeier et al. (2020) from reanalysis data and observations for the same time period (1979–2005). Fu et al. (2019) use satellite observations of stratospheric temperatures to estimate an acceleration of the mean BDC by 1.7 % per decade between 1980–2018 but a recent deceleration between 2000–2018. This is consistent with tropical lower-stratospheric temperature trends close to zero within this period, inferred by Zou et al. (2023) from reanalyses data. The temperature reduction in the tropical tropopause region and at the cold point reported for the time period 1979–2005 by Tegtmeier et al. (2020) is consistent with increased tropical upwelling. However, different reanalyses often show a significant spread when compared, whether in terms of, e.g., temperature trends in the TTL region (e.g., Tegtmeier et al., 2020) or dynamical tropical upwelling (e.g., Šácha et al., 2024).

All in all, the thermodynamic structure of the lowermost stratosphere can be expected to change in response to increasing greenhouse gas concentrations and the recovery of stratospheric ozone (e.g., IPCC et al., 2023; Charlesworth et al., 2023). This study investigates the effect of long-term changes in the tropopause and the lower-stratospheric potential temperature structure and their impact on the mass of the lowermost stratosphere on the basis of reanalysis data for the time period 1979–2019. We compare results from five modern reanalyses: ERA5, ERA-Interim, MERRA-2, JRA-55 and JRA-3Q. To illustrate our metrics for examining the LMS structure, we present results for ERA5 before generalizing our findings for all data sets. We focus on the time period after 1998, which marks the anticipated beginning of stratospheric ozone recovery.

The data and regression model used for this study are described in Sect. 2. Thereafter, Sect. 3 presents and discusses the results, divided into subsections concerning the temporal evolution of the tropopause (Sect. 3.1) and the lower-stratospheric potential temperature structure (Sect. 3.2) as well as the mass of the lowermost stratosphere (Sect. 3.3). Section 3.3 is further divided into a consideration of the LMS boundary surfaces, an LMS climatology and LMS mass trends between 1998–2019. The final conclusions are presented in Sect. 4.

2 Data and methods

2.1 Data

Reanalysis data sets are valuable assets for studying atmospheric features from process to quasi-climatological scales. In the UTLS, we know that differences exist between the various reanalyses and observations (SPARC, 2022). We therefore conduct our analysis for five reanalyses, four of which have been widely used in recent years, i.e., ERA5 (Hersbach et al., 2020), ERA-Interim (Dee et al., 2011b), MERRA-2 (Gelaro et al., 2017) and JRA-55 (Kobayashi et al., 2015), as well as the recently published JRA-3Q (Kosaka et al., 2024). For the introduction and illustration of our metrics for assessing the structure of the LMS, we use ERA5 before we generalize our findings to the other data sets.

We use ERA5 monthly mean data for the time period 1979–2019 (Hersbach et al., 2020), with 1979 marking the beginning of the satellite era. For the time period 2000–2006, the sub-reanalysis ERA5.1 replaces ERA5, correcting the reanalysis for a cold bias in the lower stratosphere (Simmons et al., 2020). We calculated the monthly mean

data and the associated standard deviations from the hourly available ERA5 data. ERA5 has 137 hybrid sigma–pressure model levels in the vertical. ERA5 thus has the finest vertical resolution among modern reanalyses. In addition to the model-level data, ECMWF provides model-level data interpolated onto 37 pressure levels between 1000 and 1 hPa. On pressure levels, the vertical grid spacing of ERA5 in the UTLS is 25 to 50 hPa, which corresponds to roughly 600–1200 m. Furthermore, model-level data interpolated on the 2 PVU surface are available from ECMWF directly (Hersbach et al., 2020). We use ERA5 data on pressure levels and 2 PVU on a regular horizontal grid with a constant grid spacing of 0.25° in longitude and latitude.

In addition, we use monthly mean data from ERA-Interim (Dee et al., 2011b), MERRA-2 (Gelaro et al., 2017), JRA-55 (Kobayashi et al., 2015) and JRA-3Q (Kosaka et al., 2024) for the same time period as ERA5. However, ERA-Interim is only available until 2018, and the MERRA-2 time series begins in 1980. We use all data on the provided pressure levels and regular horizontal grids. ERA-Interim provides 23 pressure levels, with the same spacing as ERA5 in the UTLS, interpolated from 60 hybrid sigma–pressure model levels and a horizontal grid spacing of 0.75° latitude × 0.75° longitude. MERRA-2 comes with 42 pressure levels from 72 model levels and a horizontal grid of 0.5° × 0.625°. JRA-55 contains 37 pressure levels from 60 model levels and a horizontal grid of 1.25° × 1.25°. JRA-3Q provides 40 pressure levels from 100 model levels and a horizontal grid of 1.25° × 1.25°. Table 1 presents an overview of the vertical pressure levels available in the UTLS across the different reanalyses. A more detailed comparison of the vertical levels across the reanalysis can be found in SPARC (2022) and JMA (2022).

2.2 Tropopause detection

To determine the lapse rate tropopause according to WMO (1957) from all five reanalysis data sets, we apply an algorithm closely following that of Birner (2010a), based on the work of Reichler et al. (2003). The algorithm computes the temperature lapse rate on $p^{\kappa} = p^{R_d/c_p}$ half levels (where p is the pressure, R_d is the specific gas constant and c_p is the heat capacity at constant pressure for dry air), according to Eqs. (1)–(4) in Reichler et al. (2003). Subsequently, the algorithm identifies the lowest half level at which the lapse rate becomes smaller than 2 K km^{-1}. Following Birner (2010a), a preliminary tropopause is then identified by linear interpolation of p^{κ} and all other variables to a lapse rate of exactly 2 K km^{-1} (stratification threshold). Second, the algorithm checks whether the lapse rate remains on average below 2 K km^{-1} for all higher levels within 2 km (thickness criterion). Therefore, a temporal level at a 2 km distance to the preliminary tropopause is added, and the algorithm successively checks the average lapse rate for all levels between the preliminary tropopause and 2 km distance. If the preliminary tropopause does not fulfill the thickness criterion, the next higher half level fulfilling the stratification threshold is tested. The search range is limited to 500–75 hPa to avoid unreasonable values, for example due to surface inversions. At high latitudes, especially over the Antarctic continent in austral winter, it can be difficult to obtain a meaningful lapse rate tropopause due to weak stratification (Zängl and Hoinka, 2001). We therefore limit the tropopause pressure at latitudes $> 50°$ to a minimum pressure of 150 hPa. If the detected tropopause pressure falls below this limit, the thickness criterion is suspended and the highest pressure (< 500 hPa) corresponding to a lapse rate of 2 K km^{-1} represents the tropopause. Missing values are filled by bilinear interpolation.

In addition to the thermal tropopause, we present an analysis of the dynamical tropopause in ERA5. ECMWF provides ERA5 model-level data interpolated onto the 2 PVU isosurface, which serves as the dynamical tropopause for this study. The 89 hPa isobar is taken as the tropopause cap for cases when 2 PVU is at a lower pressure than 89 hPa to avoid unreasonably large altitudes for the tropopause toward the Equator (Hersbach et al., 2020; ECMWF, 2016). Not all reanalyses provide data on the 2 PVU level or a potential vorticity variable in general. As the consistency of the dynamical tropopause across the reanalyses is therefore not guaranteed, we present trends regarding the 2 PVU tropopause only for ERA5 as an example.

Between 20° N–20° S, the cold point serves as an alternative metric to estimate the tropical tropopause (Holton et al., 1995). To deduce the cold point tropopause from all five reanalyses, we determine pressure and potential temperature at the level corresponding to a lapse rate of 0 K km^{-1}.

2.3 LMS mass

In order to determine the LMS mass, appropriate LMS boundary surfaces have to be defined. The tropopause serves as the lower boundary. For the upper LMS boundary, unlike most approaches, we do not only use a fixed isentropic value. Instead, in this study, the upper LMS boundary surface depends on the potential temperature at the tropical tropopause. Therefore, we determine the pressure at the isentrope corresponding to the mean potential temperature at the tropical (10° N–10° S) lapse rate tropopause (PPT10mean) and at the cold point (PPTcp10mean) for every time step. In many LMS studies, the 380 K isentrope has been used to approximate the upper LMS edge (e.g., Appenzeller et al., 1996; Wang and Fu, 2021). In this study, we compare 380 K with the dynamically defined upper boundaries (PPT10mean and PPTcp10mean).

The lateral LMS boundary in this study is defined as the latitude at which the respective monthly mean tropopause intersects with the 350 K isentrope. This intersection is determined by the sign change in the pressure difference between the tropopause and the isentrope. The latitude of the intersection between the tropopause and 350 K roughly marks the

Table 1. Overview of the vertical pressure levels available in the UTLS across the reanalyses used in this study.

Data set	UTLS pressure levels [hPa]														
ERA5	50	70		100	125	150	175	200	225	250	300	350	400	450	500
ERA-Interim	50	70		100	125	150	175	200	225	250	300	350	400	450	500
MERRA-2	50	70		100		150		200		250	300	350	400	450	500
JRA-55	50	70		100	125	150	175	200	225	250	300	350	400	450	500
JRA-3Q	50	70	85	100		150	175	200	225			350	400		500

location of the subtropical jet stream (e.g., Manney et al., 2011; Gettelman et al., 2011). Specifically, at 350 K, the lapse rate tropopause and the 2 PVU surface are near the isentropic PV-gradient tropopause, a transport barrier separating the extratropical lower stratosphere from the tropical troposphere (Kunz et al., 2011; Turhal et al., 2024). The isentropic PV-gradient tropopause for the time period 1979–2019 was derived according to Turhal et al. (2024) and interpolated to pressure and potential temperature fields between 50° N–50° S to be directly comparable to the lapse rate tropopause and 2 PVU.

Following Appenzeller et al. (1996), the LMS mass $M(t)$ is obtained from the three-dimensional integral of the pressure differences between the tropopause $p_1(\lambda, \Phi, t)$ and the pressure at the upper boundary $p_2(\lambda, \Phi, t)$ at every grid point and time step:

$$M(t) = \int_0^{2\pi} \int_{\Phi_1(\lambda,t)}^{\Phi_2(\lambda,t)} \int_{p_1(\lambda,\Phi,t)}^{p_2(\lambda,\Phi,t)} -\frac{1}{g} \mathrm{d}p \cos\Phi \mathrm{d}\Phi \mathrm{d}\lambda, \quad (1)$$

where g is the gravity constant, λ is the longitude, Φ is the latitude and $\mathrm{d}p$ is the pressure difference. $\Phi_1(\lambda, t)$ and $\Phi_2(\lambda, t)$ denote the lateral boundaries, defined by the intersection between the tropopause and the 350 K isentrope for every longitude and time step. All five reanalyses are used to calculate the LMS mass with respect to the lapse rate tropopause as the lower LMS boundary. For ERA5, the 2 PVU dynamical tropopause is also used.

2.4 Regression tools

We use the dynamic linear regression model (DLM) by Laine et al. (2014) for the time series analyses in this study. The DLM has proved to be useful for trend estimation in many studies (Laine et al., 2014; Ball et al., 2017, 2018, 2019; Karagodin-Doyennel et al., 2022; Bognar et al., 2022; Minganti et al., 2022) due to its ability to identify non-linear trends, smoothly varying in time without prior specification of possible inflection dates. Another strength of DLM is the rigorous treatment of uncertainties in the data and the regression coefficients by simultaneously estimating all model components. These model components include a non-linear background trend, a seasonal cycle composed of a 6- and 12-month period and an autoregressive process. The user is able to add regressor variables, assessing causes of natural variability. For the DLM trend analyses in this study, we use regressors to account for the El Niño–Southern Oscillation (NOAA), the quasi-biennial oscillation at 30 and 50 hPa (FU-Berlin), and stratospheric (volcanic) aerosol optical depth (SAOD) (Thomason et al., 2018). The same regressors have been used in different studies investigating changes in UTLS characteristics (e.g., Seidel and Randel, 2006; Meng et al., 2021; Tegtmeier et al., 2020; Zou et al., 2023). All regressors are normalized and, except for SAOD, centered around zero. In order to assess the robustness of the trends and the effect of the regressors, we conducted sensitivity tests in which the DLM was run with and without regressors. Overall, the results showed no strong dependency on the regressors used. However, tropical tropopause pressure trends, for example, become more significant when regressors are used (Figs. 2, A2).

The DLM is a Bayesian model based on the principles of Kalman filtering. The algorithm estimates the future system state based on previous estimates and the variance of the underlying data. The DLM uses an iterative process based on the Markov chain Monte Carlo (MCMC) method to infer possible system state time series from the Kalman algorithm outputs. Further details on the DLM can be found in Laine et al. (2014). The Python-based model code (dlmmc) is publicly available (Alsing, 2019). In this study, the DLM runs provide 2000 possible model state estimates after an additional 1000 samples that are considered to be warm-ups and discarded. Sensitivity experiments conducted as part of this study have shown that increasing the number of DLM samples (to, e.g., 10 000) does not significantly improve the results but comes at a considerable computational cost (see for example Fig. A1). The focus is on the hidden mean trend estimates. In the following, the DLM mean trend state time series is referred to as DLM trend state. The terms "trend" and "change" denote the DLM trend state difference between two dates, usually between January 1998 and December 2019. The fraction of DLM samples resulting in a negative (positive) change between two dates serves as an evaluation of the confidence of the trend. The use of the term "statistical significance" refers to the probability of an overall decrease (increase) $> 95\,\%$ instead of frequentist significance tests. Ball et al. (2018, 2019) use this approach to evaluate their ozone trend analysis.

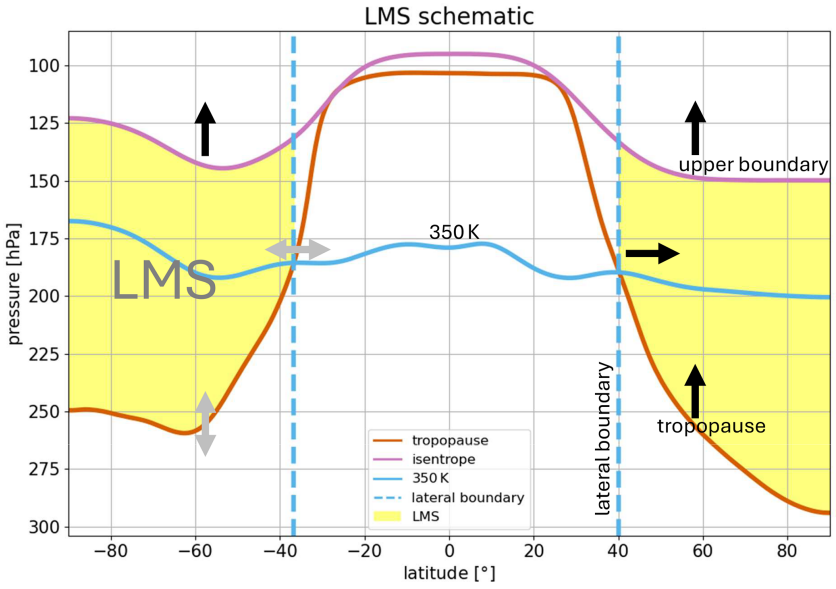

Figure 1. Schematic of the LMS. The LMS mass is enclosed by a lower boundary (tropopause, red), an upper boundary (purple) and a lateral boundary (vertical blue lines). The lateral boundary in this study is defined as the intersection between the tropopause and the 350 K isentrope, approximating the location of the subtropical jet streams and the maximum PV gradient, marking a transport barrier. The arrows indicate the long-term changes in the boundary surfaces, affecting the LMS mass as presented in Sect. 3.1 and 3.3.1. Figure 8 shows the location of the different LMS boundary surfaces compared in this study.

3 Structural changes in the lowermost stratosphere based on reanalysis data

3.1 Temporal evolution of the tropopause

Figure 2 shows the DLM trend results over the period 1998–2019 for the zonal mean tropopause pressure (upper panels), potential temperature (middle row) and geopotential height (lower panels) in ERA5. In the NH mid-latitudes, both the ERA5 lapse rate tropopause and the 2 PVU dynamical tropopause show negative pressure trends of around −1 hPa per decade (Fig. 2a and b). This pressure decrease corresponds to a lifting of the tropopause (Fig. 2g and h) and is consistent with the positive potential temperature trends (Fig. 2d and e). ERA-Interim, MERRA-2, JRA-3Q and JRA-55 exhibit remarkably similar lapse rate tropopause trends, which enhances the robustness of the findings (Fig. 3a and c). Furthermore, similar tropopause trends have been reported by Wilcox et al. (2012) for the time period 1989–2007 and Meng et al. (2021) for the time period 1980–2020.

The tropical and subtropical lapse rate tropopause in ERA5 exhibits statistically significant upward trends accompanied by negative trends in pressure (ca. −0.5 hPa per decade, Fig. 2a and g) and more pronounced potential temperature trends compared to the extratropics (ca. 0.7 K per decade, Fig. 2d). Since the 2 PVU tropopause is capped at a fixed pressure of 89 hPa in the tropics, the respective pressure trends in the inner tropics are not meaningful (Fig. 2b, e and h). As Fig. 2c and i reveal, the zonal mean cold point in ERA5 is rising, accompanied by a statistically significant pressure decrease of on average −0.7 hPa per decade (Fig. 2c), which is in agreement with the findings of Tegtmeier et al. (2020). The upward tendency of the cold point in ERA5 is joined by a potential temperature increase of on average 1 K per decade (Fig. 2f). All considered reanalyses agree on negative pressure trends at the tropical lapse rate tropopause and the cold point (Fig. 3a and b), whereas potential temperature trends differ in sign (Fig. 3c and d). Specifically, while ERA5, ERA-Interim and MERRA-2 agree on positive potential temperature trends between 10° N–10° S, JRA-3Q and JRA-55 suggest the opposite. These discrepancies can be attributed to contrasting absolute temperature trends in the TTL region suggested by the reanalyses, such as those visible at the 100 hPa pressure level (Fig. 4).

SH tropopause trends are less conclusive than in the NH. Within ERA5, lapse rate and 2 PVU dynamical tropopause pressure trends differ in sign at most latitudes (Fig. 2a and b). The ERA5 SH mid-latitude lapse rate tropopause generally shows positive pressure trends ranging between 0 and +2 hPa per decade, corresponding to a sinking of the tropopause (Fig. 2a and g), while 2 PVU pressure trends in this region amount to around −0.8 hPa per decade (Fig. 2b). Throughout the reanalyses, lapse rate tropopause trends show a large spread in the SH extratropics (Fig. 3a and c). Like in ERA5, a positive pressure trend in the SH mid-latitude lapse rate tropopause between 30–40° S is also evident in ERA-Interim, MERRA-2 and JRA-55 but not in JRA-3Q (Fig. 3a). A sim-

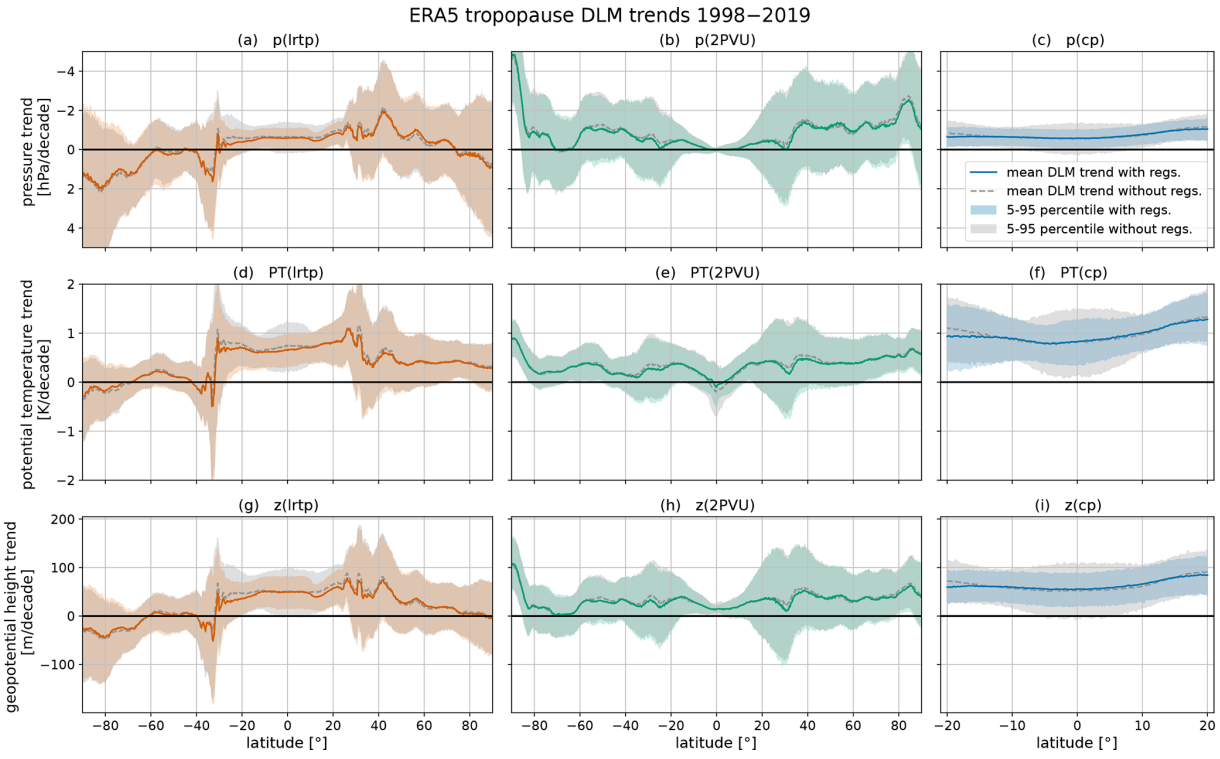

Figure 2. Zonal mean tropopause pressure **(a, b, c)**, potential temperature **(d, e, f)** and geopotential height **(g, h, i)** trends between 1998–2019 as estimated by the DLM from ERA5 data. Note that the pressure trend axis is inverted because decreasing pressure is associated with an upward trend in the pressure coordinate system. The lines show the mean DLM trends, and the shading denotes the 5th–95th percentiles. DLM results including regressors are presented as solid lines and in color; DLM results without regressors are shown as dashed lines and in gray. Red is associated with the lapse rate tropopause **(a, d, g)**, green **(b, e, h)** indicates the 2 PVU dynamic tropopause (capped at 89 hPa in the tropics) and blue **(c, f, i)** indicates the cold point.

ilar tropopause behavior has been observed by Xian and Homeyer (2019) for the reanalyses JRA-55, MERRA-2 and CFSR. On the other hand, Xian and Homeyer (2019) do not observe such a downward trend in the SH mid-latitude lapse rate tropopause in ERA-Interim and the downward trend seems to oppose the findings by Wilcox et al. (2012) and Meng et al. (2021). However, it has to be noted that in this study, we focus on tropopause changes after 1998. The non-linear DLM trend analysis for the entire time series of 1979–2019 reveals a trend reversal of the ERA5 lapse rate tropopause pressure around the year 2000. This trend reversal is evidenced by the fact that the DLM pressure trend state reaches its minimum around the year 2000 (Fig. 5). Accordingly, the DLM results suggest decreasing pressure of the ERA5 SH mid-latitude lapse rate tropopause before the year 2000 and increasing pressure thereafter. The DLM trend state of 2 PVU and cold-point pressure can be found in the Appendix (Fig. A3).

In the polar regions of both hemispheres, ERA5 suggests increasing tropopause pressure, which is evident in most reanalyses and highly significant in the SH in JRA-3Q and JRA-55 (Figs. 2a and 3a). The positive pressure trends at the lapse rate tropopause above high latitudes could be the result of polar ozone recovery and associated increasing temperatures in the polar lower stratosphere (LS) after 1998. This is consistent with the minimum lapse rate tropopause pressure DLM trend state in the polar regions, estimated around the time of ozone trend reversal (around the year 2000) (Fig. 5). A descent of the SH polar lapse rate tropopause has also been observed by Wilcox et al. (2012) and in some of the reanalyses analyzed by Xian and Homeyer (2019). Moreover, the downward trend in the lapse rate tropopause at high and mid-latitudes could be linked to an acceleration of the BDC (Birner, 2010b). Indeed, the age of air and long-lived trace gas measurements indicate an accelerating BDC in the SH after around the year 2000 (Strahan et al., 2020; Ploeger and Garny, 2022).

3.2 Temporal evolution of the lower-stratospheric potential temperature structure

In addition to trends in the tropopause location, the location of isentropic surfaces is an important measure of structural changes in the UTLS region. Using ERA5 as an example, Fig. 6a–c show the pressure trend on isentropes at 380, 400 and 430 K for the time period 1998–2019 as estimated by

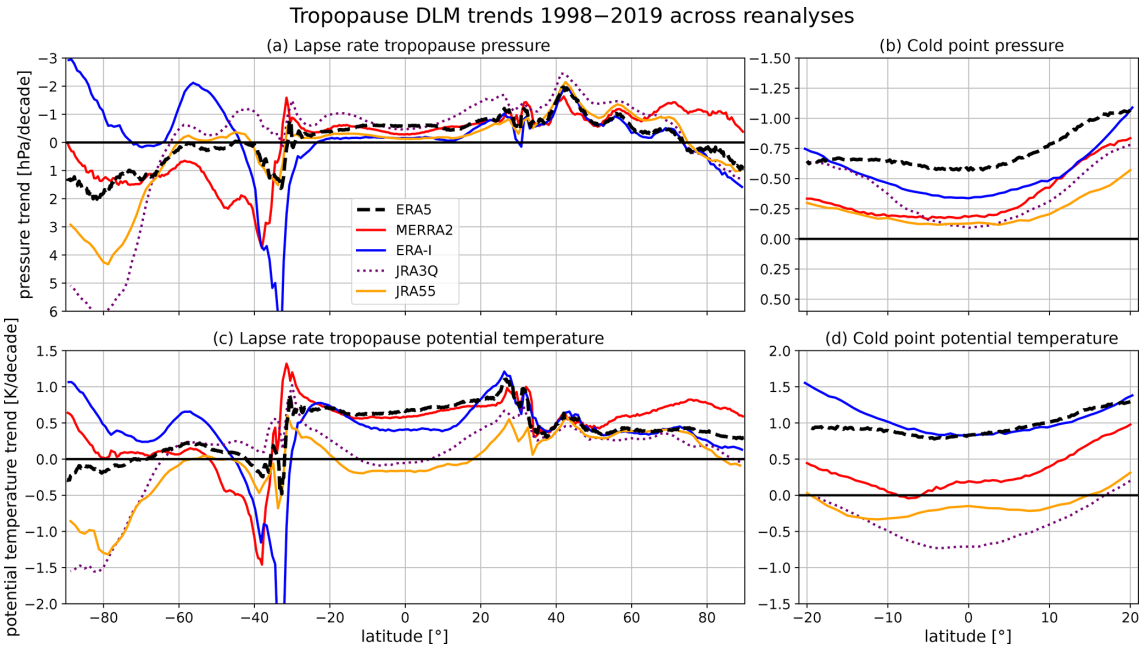

Figure 3. Zonal mean lapse rate tropopause **(a, c)** and cold-point **(b, d)** trends between 1998–2019 as estimated by the DLM from different reanalyses. The reanalyses compared are ERA5 (black, dashed), MERRA-2 (red, solid), ERA-Interim (blue, solid), JRA-3Q (purple, dotted) and JRA-55 (orange, solid). The upper panels display pressure trends, and the lower panels show potential temperature trends. Note that the pressure trend axis is inverted because decreasing pressure is associated with an upward trend in the pressure coordinate system. The lines show the mean DLM trends. For the sake of clarity, the presentation of uncertainty has been omitted but is of the same order of magnitude as in Fig. 2a, c, d and f.

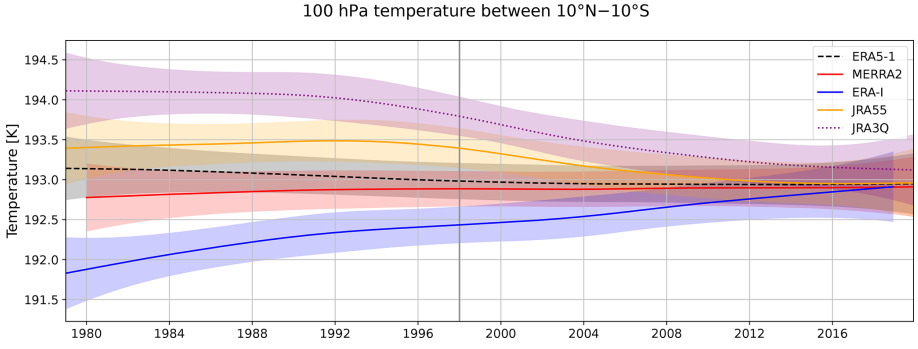

Figure 4. DLM trend state for the average tropical (10° N–10° S) temperature at 100 hPa in ERA5 (black, dashed), MERRA-2 (red, solid), ERA-Interim (blue, solid), JRA-55 (orange, solid) and JRA-3Q (purple, dotted) for the time period 1979–2019. Shading denotes the range of 2 standard deviations. The ERA-Interim time series ends in 2018, and MERRA-2 begins in 1980.

the DLM. The average pressure trends range between −0.3 and +0.6 hPa per decade, which corresponds to an absolute pressure change of up to 1 hPa during the 21-year period, though with large uncertainties, especially in the extratropics. The pressure trends between 380–430 K are positive in the extratropics. In the tropics and subtropics, on the other hand, the pressure for the isentropes above 380 K is found to be decreasing, which is accompanied by a rise of the respective potential temperature isosurfaces in geopotential height (Fig. A4a). The isentropic pressure trends are hardly statistically significant but robust within the reanalyses (except ERA-Interim) (Fig. 6d–f). However, while the 380 K isentrope in ERA5 and MERRA-2 shows no pressure trend in the tropics and subtropics, JRA-55 and JRA-3Q show a significant pressure decrease (Fig. 6d). Decreasing pressure of lower-stratospheric isentropes in the tropics and increasing pressure in the extratropics are consistent with a strengthened BDC, which is associated with adiabatic cooling in the tropical LS and warming in the extratropical LS.

The magnitude of the isentropic pressure trend for a given latitude bin varies at different potential temperatures. In the tropics and subtropics in ERA5, higher isentropes are ris-

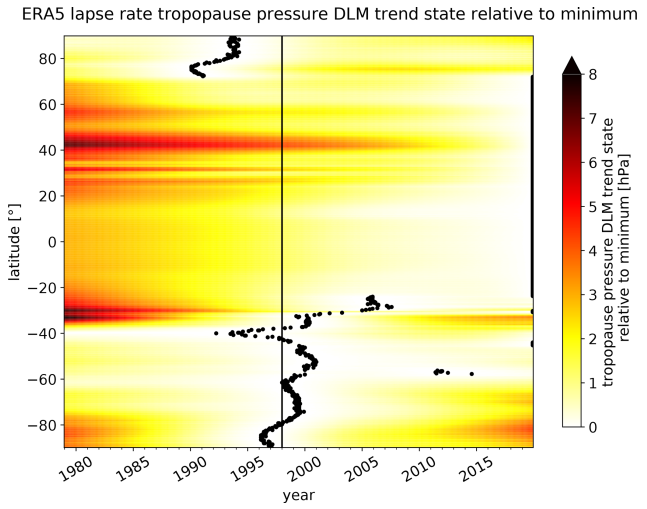

Figure 5. DLM trend state time series of pressure at the lapse rate tropopause in ERA5 for the time period 1979–2019. The panels show the pressure trend state time series for all latitudes (y axis). The minimum pressure trend state for every grid point is highlighted by the black dots and can indicate a trend reversal from decreasing to increasing pressure. The trend state time series are presented relative to the respective minimum but in absolute numbers (hPa) (color shading). The vertical black line marks the beginning of the year 1998.

ing at a faster rate than lower ones (Fig. 6a–c). This indicates a weakening of the potential temperature gradient with pressure and accordingly a change in the stratification in the lower stratosphere. Such lower-stratospheric isentropic pressure trends could potentially be linked to TIL changes (e.g., Gettelman and Wang, 2015; Boljka and Birner, 2022), at least in the tropics. However, this behavior is only evident in the ECMWF reanalyses (Fig. 6d–f). While the average pressure changes discussed in this paragraph provide valuable insights, examining the full, non-linear DLM trend state time series can offer a more comprehensive view of the physical mechanisms driving trend evolution.

In addition to the average isentropic pressure trends between 1998–2019, it is worth considering the entire DLM trend state time series, as the DLM is able to identify non-linear trends. Taking ERA5 as an example, the DLM estimates a trend reversal from decreasing to increasing pressure at isentropes between 380–430 K in the extratropics, spread around the year 2000. This trend reversal is evident from the minimum in the DLM trend state (Fig. 7). At SH high latitudes, isentropes reach their minimum pressure trend state later, between 2006–2008, but pressure changes are most pronounced in this region. In SH high latitudes in particular, decreasing isentropic pressure between the 1980s and the 2000s is consistent with a cooling of the lower stratosphere due to ozone decline. This relationship between lower stratospheric temperatures and isentropic pressure directly follows from the definition of potential temperature. Ozone recovery leads to a warming of the stratosphere, consistent with increasing isentropic pressure in the lower stratosphere since the 2000s. This is in good agreement with the SH stratospheric temperature studies by Fu et al. (2019). In the SH high latitudes, this (potential) temperature increase is associated with a weakening of the SH polar vortex (Zambri et al., 2021), influencing polar winter ozone destruction and mixing of polar and mid-latitude air masses.

In the tropics and subtropics, continuous pressure decline accompanied by a rise in ERA5 isentropes above 380 K is evident (Fig. 7). This is consistent with increased upwelling in the context of an enhanced BDC, associated with adiabatic cooling. Furthermore, diabatic cooling of the tropical lower stratosphere can be expected from increasing GHG load in the atmosphere and a continuous decline in lower-stratospheric ozone (e.g., Ramaswamy et al., 2001; Vallis et al., 2015). Such a cooling of the tropical lower stratosphere has been identified in observations (e.g., Scherllin-Pirscher et al., 2021) and reanalysis data (e.g., Tegtmeier et al., 2020) and is consistent with our analysis.

3.3 The mass of the lowermost stratosphere

3.3.1 LMS boundary surfaces

The tropopause marks the lower boundary of the lowermost stratosphere (LMS). For the upper boundary, many studies choose the 380 K isentrope (e.g., Appenzeller et al., 1996; Wang and Fu, 2021). Wang et al. (2022) point out the importance of considering long-term changes in the tropical tropopause location in different climates for LMS mass budget analyses. Their approach is to fit an isentrope between 360–390 K to the tropical lapse rate tropopause. Similar to Wang et al. (2022), we define an upper LMS boundary with respect to the tropical lapse rate tropopause that allows for continuous variations in the boundary surface. To do so, we determine the mean isentropic pressure corresponding to the potential temperature at the tropical (10° N–10° S) lapse rate tropopause (PPT10mean). For comparison, we determine a second upper-boundary surface based on the potential temperature at the cold point (PPTcp10mean) in the same way. The locations of the different boundary surfaces used for LMS definition are displayed in Fig. 8 using ERA5 as an example.

As is evident from Figs. 9 and 10, a fixed upper LMS boundary (e.g., 380 K) cannot capture the variability and long-term evolution associated with the tropical tropopause. Specifically, in ERA5, the dynamically defined upper-boundary surfaces (PPT10mean and PPTcp10mean) show an opposite trend to the 380 K isentrope (Fig. 9a–c). This is due to the fact that the potential temperature at the tropical tropopause exhibits a positive trend (Fig. 9d). For the mean potential temperature at the ERA5 lapse rate tropopause between 10° N–10° S, the DLM estimates an increase of 1.33 ± 0.40 K between 1998–2019. The temporal

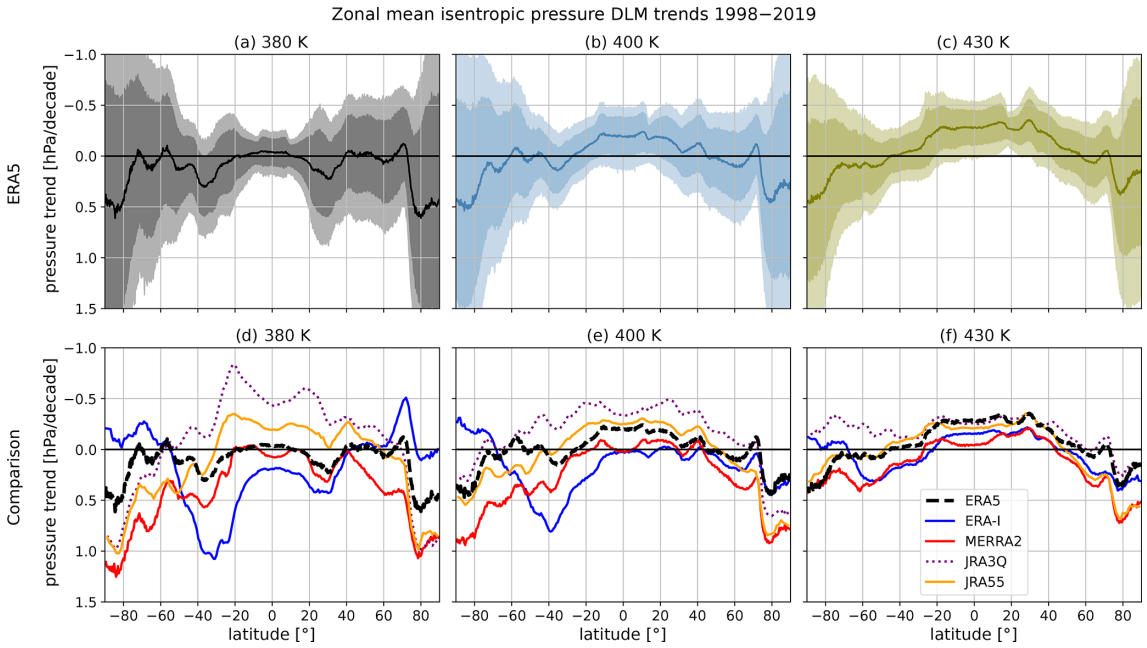

Figure 6. Zonal mean pressure trends at the 380 K **(a, d)**, 400 K and **(b, e)** 430 K **(c, f)** isentropes as estimated by the DLM for the time period 1998–2019. As an example, ERA5 isentropic pressure trends are depicted in the upper panels, showing the mean trend (solid line) together with the associated standard deviation (dark shading) and the 5th–95th percentiles. The lower panels compare results for the different reanalyses, i.e., ERA5 (black, dashed), MERRA-2 (red, solid), ERA-Interim (blue, solid), JRA-3Q (purple, dotted) and JRA-55 (orange, solid). For the sake of clarity, the presentation of uncertainty has been omitted in the lower panels. Note that the pressure trend axis is inverted because decreasing pressure is associated with an upward trend in the pressure coordinate system. The trends are given in hectopascals per decade.

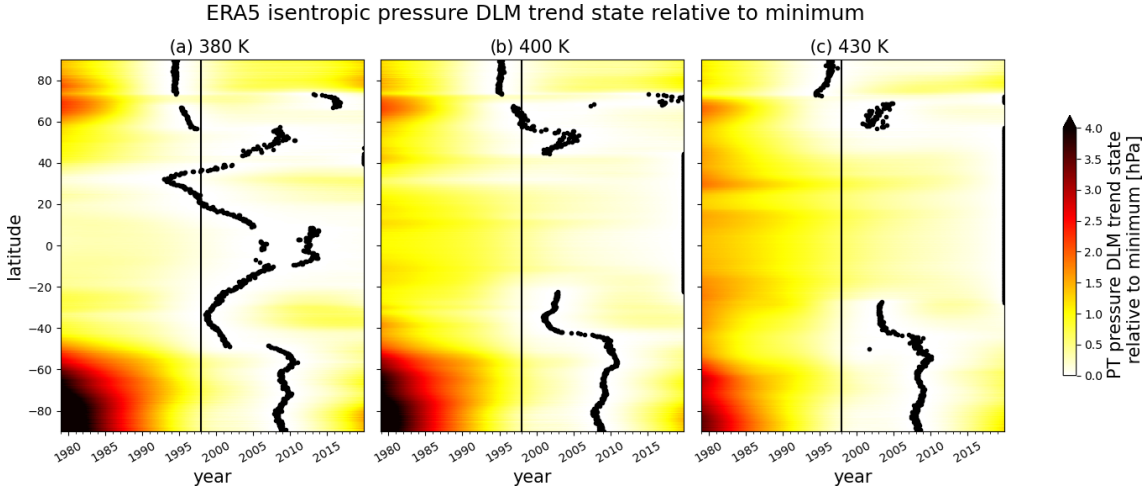

Figure 7. Isentropic pressure DLM trend state time series for the time period 1979–2019 at 380 K **(a)**, 400 K **(b)** and 430 K **(c)** in ERA5 for all latitudes (y axis). The minimum pressure trend state for every grid point is highlighted by the black dots and can indicate a trend reversal from decreasing to increasing pressure. The pressure trend state time series are presented relative to the respective minimum but in absolute numbers (hPa) (color shading). The vertical black line marks the beginning of the year 1998.

evolution of the potential temperature corresponding to the cold point amounts to 1.72 ± 0.53 K for the same time period. The potential temperature increase at the tropical tropopause leads to a global lifting of the defined upper LMS boundary surfaces in ERA5 (Fig. 9b and c). The upward trends in the PPT10mean and PPTcp10mean surfaces in ERA5 are statistically significant for most latitudes in the tropics and mid-latitudes. The average pressure trends of around -1 hPa per decade are very similar to the trend of the 2 PVU tropopause and the lapse rate tropopause in the NH mid-latitudes (Fig. 2a

and b). In the SH extratropics, the sign of the lapse rate tropopause pressure trend is opposite to that of the PPT surfaces. Like in ERA5, a significant rise in the PPT10mean surface in the extratropics is also evident in ERA-I and MERRA-2 (Fig. 10b). This can be attributed to the increase in tropical tropopause potential temperatures, which define the isentropes corresponding to PPT10mean (Fig. 10d). On the other hand, JRA-55 and JRA-3Q suggest the opposite (Fig. 10b and d). At the cold point, ERA5 and ERA-Interim agree on continuously increasing potential temperatures between 1998–2019, whereas the JRA data sets show mostly decreasing potential temperatures and MERRA-2 almost no trend at all (Fig. 10e). This is reflected in the trends in the PPTcp10mean surface (Fig. 10c). The contrasting behavior of the reanalyses can at least partly be attributed to the respective temperature trends in the TTL region. As is evident from Fig. 4, ERA5 and MERRA-2 suggest no temperature trend at 100 hPa between 1998–2019, whereas temperatures in JRA-55 and JRA-3Q decrease by -0.4 ± 0.2 K and -0.7 ± 0.2 K, respectively. In ERA-Interim, temperatures at 100 hPa increase significantly after 1998. For the LMS mass analysis in Sect. 3.3.2 and 3.3.3, we use 380 K, PPT10mean and PTcp10mean as upper LMS boundaries and compare their respective effects on the LMS mass. The different trends in the isosurfaces discussed here are reflected in the LMS mass trends.

Like the upper and lower LMS boundaries, the boundaries separating the LMS laterally from the TTL region are allowed to vary dynamically with time. For this purpose, the intersections between the monthly mean tropopause and the 350 K isentrope are identified via the sign change in the pressure difference between both surfaces. This intersection serves as a proxy for the position of the subtropical jet stream (e.g., Manney et al., 2011; Gettelman et al., 2011). Specifically, the lapse rate tropopause and the 2 PVU surface at 350 K are close to the isentropic PV-gradient tropopause (Fig. 8), which marks a clear transport barrier between the tropical troposphere and the extratropical lower stratosphere, i.e., the LMS (Kunz et al., 2011; Turhal et al., 2024). For comparison, the intersections of the tropopause with isentropes between 330–370 K are also determined. The 380 K isentrope often does not intersect with the respective tropopause, which is why it is not further considered. The zonal mean latitudes of the intersection between the lapse rate (2 PVU) tropopause and the 350 K isentrope, i.e., the lateral LMS boundaries in ERA5, vary between 29–48° N (26–40° N) and 31–45° S (26–36° S), with the lapse rate tropopause intersection always poleward of the 2 PVU intersection. Other definitions of the lateral LMS boundaries have been used in the literature, such as the intersection between the respective upper and lower LMS boundary surfaces (Appenzeller et al., 1996; Hegglin et al., 2010) or the zero diabatic heating rate at the upper LMS boundary surface (Wang and Fu, 2021; Wang et al., 2022). We consider the latitude of the intersection between the tropopause and the 350 K isentrope to be a practical approximation of the location of the physical transport barrier between the (extratropical) LMS and the tropical troposphere, marked by the isentropic PV-gradient tropopause.

Besides the seasonal variability, the DLM identifies a trend in the intersections between the tropopause and 350 K isentrope, as shown in Fig. 11. Here, the intersections of the zonal mean tropopause and isentropes are considered. In the NH, this trend is directed poleward for the lapse rate tropopause in all reanalyses (Fig. 11b) and 2 PVU in ERA5 (Fig. A5b). Such a poleward tendency is also evident for intersections of the NH tropopause with isentropes at 360 and 370 K, which indicates an expansion of the NH tropics. The results are robust across all examined reanalyses and consistent with evidence of a widening of the tropical belt, reported in many studies (e.g., Birner, 2010a; Wilcox et al., 2012; Xian and Homeyer, 2019). Our metric and findings are similar to other metrics based on cross-points between isentropic and potential vorticity fields (Juan Antonio Añel, personal communication, 2018).

In the SH, on the other hand, the lateral tendencies of the intersections between the tropopause and isentropes are less clear. For the lapse rate tropopause at 350 K, all reanalyses except JRA-3Q agree on an equatorward trend, though they differ in magnitude and statistical significance. In contrast to the lapse rate tropopause, the 2 PVU dynamical tropopause in ERA5 shows a poleward trend at 350 K (Fig. A5a). However, the general shape of the lateral tropopause trends with respect to potential temperature is similar in most reanalyses (Fig. 11a) and has also been found for the PV-gradient tropopause by Turhal et al. (2024). The different magnitudes of the lateral trends for tropopause intersections with different isentropes suggest a shape change in the subtropical tropopause. The larger poleward tendency of the tropopause around 370 K, as is evident in ERA5, JRA-55 and JRA-3Q, hints at a steeper tropopause. This could be associated with higher zonal wind speeds, i.e., an intensification of the subtropical jet (Manney and Hegglin, 2018; Maher et al., 2020). Furthermore, such a steepening of the subtropical tropopause, including the tropopause break, could be an indication of a strengthened BDC (Birner, 2010b). As far as the LMS mass is concerned, the temporal evolution of the lower, upper and lateral LMS boundaries points toward a trend in the LMS mass, which is addressed in Sect. 3.3.3.

3.3.2 LMS mass climatology

The mean LMS mass in ERA5 between all considered boundary surfaces on both hemispheres is listed in Table 2. In ERA5, the average global LMS mass between the different boundary surfaces (lrtp, 2 PVU and 380 K, PPT10mean, PPTcp10mean) ranges from $0.99 \pm 0.28 \cdot 10^{17}$ kg (resulting from lrtp-PPT10mean) to $1.89 \pm 0.37 \cdot 10^{17}$ kg (resulting from 2 PVU-PPTcp10mean) within the time period 1979–2019. Since the 2 PVU tropopause is located at a significantly

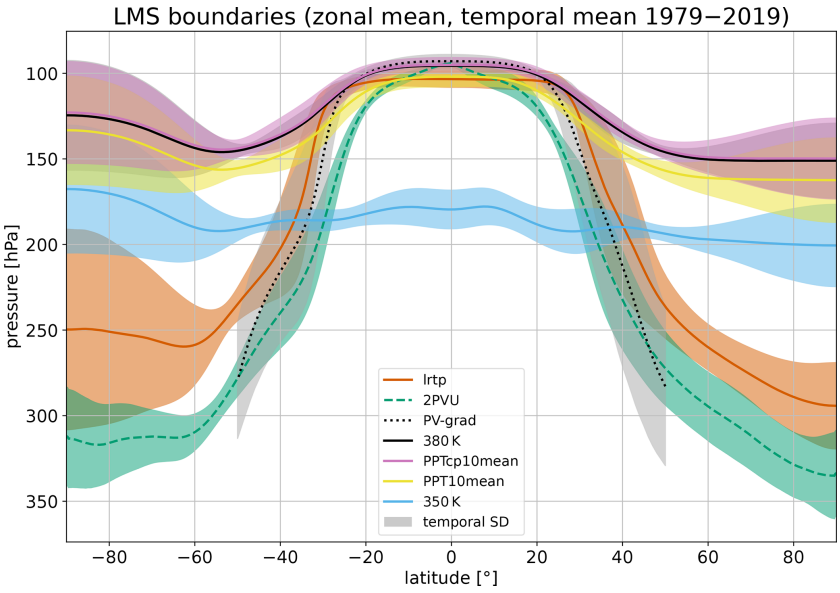

Figure 8. Zonal mean and temporal mean LMS boundaries between 1979–2019 using ERA5 as an example. The lines denote the mean location of the respective surfaces, and the shading indicates the temporal standard deviation. The lower LMS boundary is defined by the lapse rate tropopause (red) or the 2 PVU dynamic tropopause (green, dashed). The 380 K isentrope (black) can serve as the upper boundary. It is also possible to define dynamic upper boundaries depending on the potential temperature at the tropical tropopause. Here, the isentropes corresponding to the mean potential temperature between 10° N–10° S at the lapse rate tropopause (PPT10mean, yellow) and the cold point (PPTcp10mean, purple) are shown. The lateral LMS boundary can be approximated by the intersection between the 350 K isentrope (light blue) and the respective tropopause. This intersection is close to the isentropic PV-gradient tropopause (black, dotted) at 350 K, which represents a transport barrier and serves as an approximation of the position of the subtropical jet stream.

higher pressure than the lapse rate tropopause (Fig. 8), the LMS mass between 2 PVU and the respective upper boundary is 1.6–1.8 times larger than the mass with respect to the thermal tropopause. The LMS mass with respect to the different upper-boundary surfaces varies by less than 15 % for the same lower boundary and hemisphere. If the upper edge of the stratosphere is approximated at 1 hPa, the proportion of LMS mass to total stratospheric mass is about 20 %.

LMS mass values in ERA-Interim, MERRA-2, JRA-55 and JRA-3Q are very similar, and the different boundary surfaces have the same effect as in ERA5 (Table A1). The MERRA-2 LMS mass deviates the most from the other reanalyses, generally showing smaller values, but the relative differences between the data sets are smaller than 10 % in the NH and smaller than 20 % in the SH. The variations in LMS mass across the reanalyses can primarily be attributed to the differences in tropopause location, determining the lower LMS boundary and the dynamical upper boundaries (Fig. A6).

In general, the NH mean LMS mass is smaller than the SH mass, independent of the boundary surfaces. This is due to the greater seasonal variability of the LMS mass in the NH, reaching smaller minima in summer than in the SH. Within one hemisphere, low latitudes contribute considerably more to the LMS mass than high latitudes due to the area decrease from the Equator to the pole.

The LMS mass calculated in this study between the respective boundary surfaces can be compared to results reported by Appenzeller et al. (1996) and Hegglin et al. (2010) (Table 2). Using the example of ERA5, the LMS mass in this study is on average 1.5 to 4.8 times smaller than previously reported. The reason for the discrepancies is in particular the choice of the boundaries. Appenzeller et al. (1996) integrate the pressure between the 2 PVU surface and the 380 K isentrope from United Kingdom Meteorological Office (UKMO) data with a horizontal grid of 2.5° latitude by 3.75° longitude and 50 hPa in the vertical, with zonal mean daily data for the year 1993. The resulting UKMO dynamic tropopause is situated around 50–100 hPa lower than the ERA5 2 PVU surface. Hegglin et al. (2010) use NCEP National Centers for Environmental Prediction (NCEP) monthly mean and zonal mean reanalysis data for the time period 1990–1999 with a horizontal grid of 2.5° by 2.5°. They choose the thermal tropopause as the lower boundary and the 100 hPa isobar as a fixed upper boundary for the mass computation. The upper boundaries used in this study are (on average) situated between 90–187 hPa. For the lateral boundaries, Hegglin et al. (2010) and Appenzeller et al. (1996) use the intersections between upper- and lower-boundary surfaces. The lateral LMS boundaries in this study are at considerably higher latitudes. Using the same LMS boundary definitions as Hegglin et al. (2010) and ERA5 zonal mean data for the time period 1979–

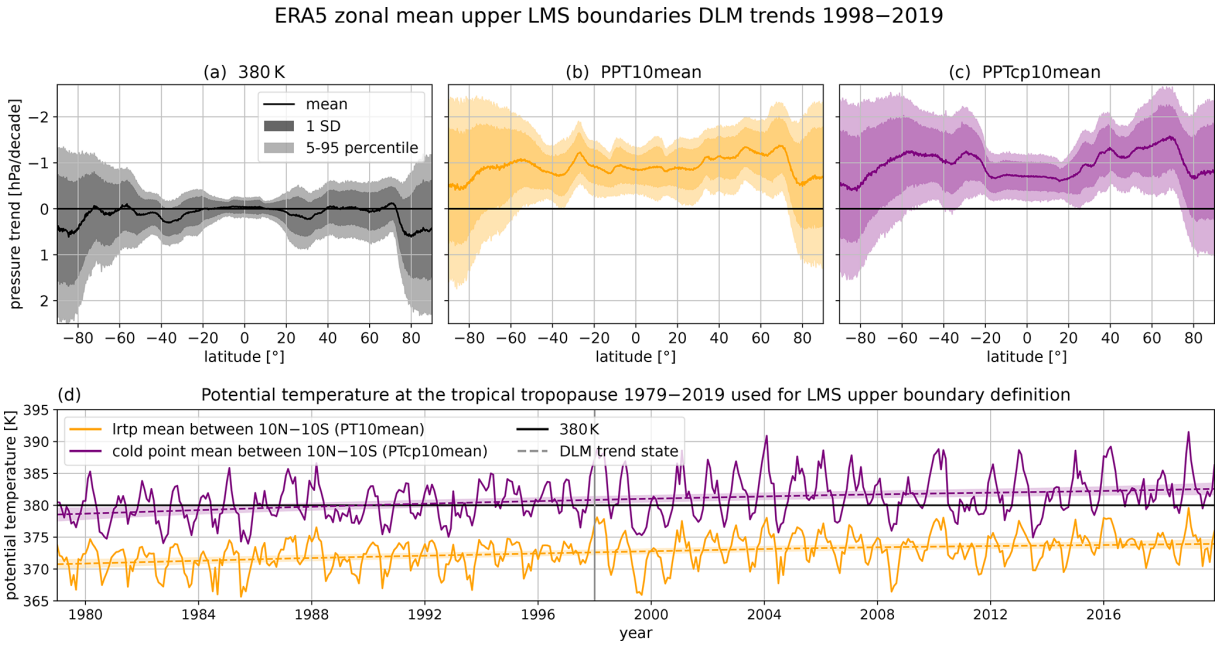

Figure 9. Zonal mean pressure trends in the LMS upper boundaries in ERA5 as estimated by the DLM for the time period 1998–2019 **(a, b, c)** together with the potential temperature evolution at the tropical tropopause **(d)**. The potential temperature at the tropical (10° N–10° S) lapse rate tropopause (PT10mean, orange) and the cold point (PTcp10mean, purple) define the isentropes that serve as dynamical upper LMS boundaries (PPT10mean and PPTcp10mean). The upper LMS boundary can also be approximated with the 380 K isentrope, which is also presented (black). In the upper panels, the pressure trends in the respective boundaries are presented, showing the mean trend (solid line) together with the associated standard deviation (dark shading) and the 5th–95th percentiles (light shading). Note that the pressure trend axis is inverted because decreasing pressure is associated with an upward trend in the pressure coordinate system. The lower panel shows the potential temperature time series (solid line) between 1979–2019 together with the DLM trend state time series (dashed lines) and the range of 2 standard deviations (shading). The vertical gray line marks the beginning of the year 1998.

Table 2. Mean LMS mass and associated standard deviation in 10^{17} kg for different LMS definitions and data. As an example for the LMS mass in this study, LMS mass from ERA5 data is averaged over 1979–2019 and rounded to the second decimal. In Fig. 5 of Appenzeller et al. (1996), daily LMS mass values from United Kingdom Meteorological Office (UKMO) data are presented for the years 1992 and 1993. Figure 6 in Hegglin et al. (2010) shows monthly mean LMS mass from National Centers for Environmental Prediction (NCEP) data averaged over the time period 1990–1999. The LMS mass values from Appenzeller et al. (1996) and Hegglin et al. (2010) in this table are estimated from the respective figures.

Study and data	LMS	NH	SH
This study			
ERA5	lrtp-PPT10mean	0.49 ± 0.20	0.50 ± 0.08
	lrtp-PPTcp10mean	0.56 ± 0.22	0.58 ± 0.09
	lrtp-380K	0.55 ± 0.20	0.57 ± 0.10
	2PVU-PPT10mean	0.80 ± 0.24	0.90 ± 0.11
	2PVU-PPTcp10mean	0.89 ± 0.25	1.00 ± 0.12
	2PVU-380K	0.88 ± 0.23	0.99 ± 0.13
Appenzeller et al. (1996)			
UKMO	2 PVU–380 K	2.3 ± 0.4	2.4 ± 0.1
Hegglin et al. (2010)			
NCEP	lrtp–100 hPa	1.6 ± 0.3	1.5 ± 0.1

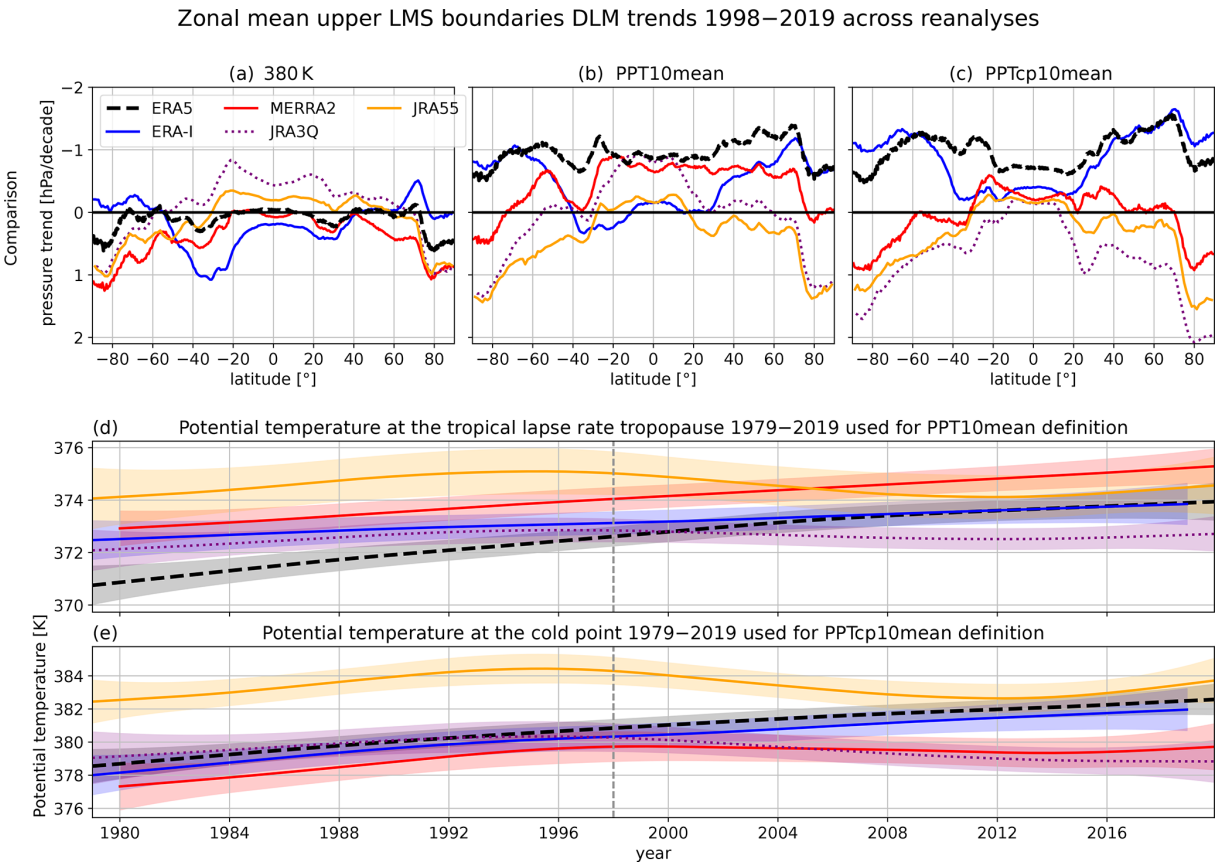

Figure 10. Similar to Fig. 9 but comparing the LMS upper-boundary evolution across the reanalyses, i.e., ERA5 (black, dashed), MERRA-2 (red, solid), ERA-Interim (blue, solid), JRA-3Q (purple, dotted) and JRA-55 (orange, solid). In the upper panels, the mean DLM pressure trends (1998–2019) in the different LMS upper boundaries, i.e., 380 K **(a)**, PPT10mean **(b)** and PPTcp10mean **(c)**, are presented. For the sake of clarity, the presentation of uncertainty has been omitted in the upper panels but is of the same order of magnitude as in Fig. 9. Note that the pressure trend axis is inverted because decreasing pressure is associated with an upward trend in the pressure coordinate system. The lower panels show the DLM trend state time series of potential temperature at the tropical (10° N–10° S) lapse rate tropopause (PT10mean, **d**) and the cold point (PTcp10mean, **e**) (solid line) between 1979–2019. Depicted are the means (lines) together with the range of 2 standard deviations (shading). The vertical gray line marks the beginning of the year 1998.

2019, we compute an average LMS mass of around $1 \cdot 10^{17}$ kg for each hemisphere. With a downward shift of the 2 PVU surface by 60 hPa, we obtain the same LMS mass as Appenzeller et al. (1996).

3.3.3 LMS mass trends

As presented in Sect. 3.1 and 3.3.1, the trends in the LMS lower, upper and lateral boundaries suggest a long-term change in the LMS mass enclosed by the respective boundary surfaces. In ERA5, the observed extratropical tropopause trends (Sect. 3.1, Fig. 2) and the lifting trend in the tropical tropopause (Fig. 9) indicate that the rise in the upper LMS boundary could potentially compensate for the rising lower boundary and the poleward transition of the lateral boundary. The results illustrated in Fig. 12a, b and d confirm this expectation. For the LMS in ERA5 bounded with 380 K, the DLM analysis results in a significant negative trend in the LMS mass between 1998–2019 (except for the LMS mass with respect to the SH lapse rate tropopause). In contrast, the LMS defined with a dynamical upper boundary based on the tropical tropopause (PPT10mean and PPTcp10mean) shows mean mass trends close to zero or even positive trends. Focusing on the latitude bins poleward of the mean lateral LMS boundary (latitude bins 50–80 and 60–90°), LMS mass changes are positive or less negative but stay significantly negative if 380 K is used as the upper boundary. This suggests three things. (1) The decreasing NH LMS mass for a fixed 380 K boundary is largely due to the rising NH extratropical tropopause. (2) The dynamical upper-boundary surfaces based on the tropical tropopause are indeed able to largely compensate for the tropopause rise in ERA5. (3) Locally, a considerable proportion of this NH LMS mass decline can be attributed to the poleward trend in the lateral boundary, which is the result of an expansion of the tropics, while the hemispheric effect is rather small. Figure 13a con-

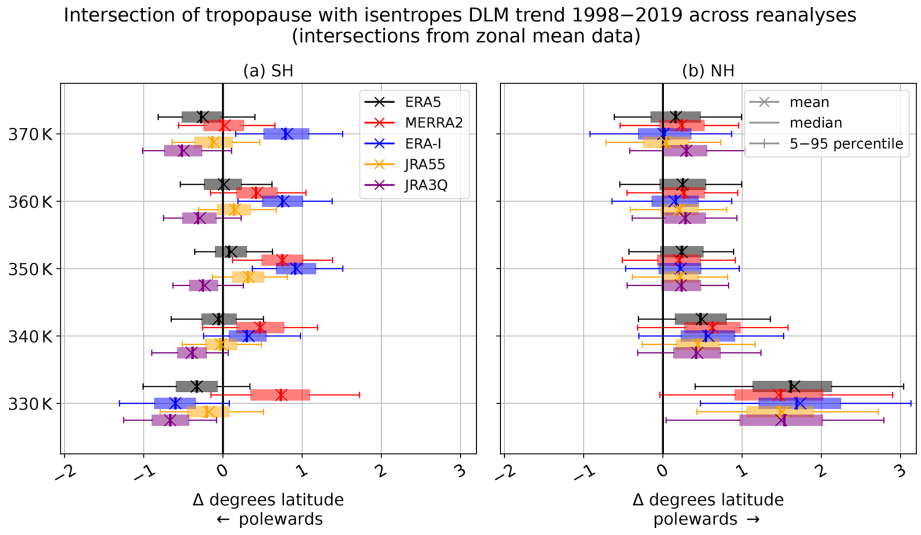

Figure 11. Trend in the latitude of intersection between the zonal mean lapse rate tropopause and isentropes between 330–370 K (y axis) for all reanalyses. The reanalyses compared are ERA5 (black, uppermost boxplot), MERRA-2 (red, second box), ERA-Interim (blue, third box), JRA-55 (yellow, fourth box) and JRA-3Q (purple, lowermost boxplot). The trends are DLM estimates for the time period 1998–2019. In the SH **(a)**, negative trends are associated with a poleward tendency, and in the NH **(b)**, positive trends indicate a poleward shift. The DLM trend estimates are presented as box-and-whisker plots.

firms these observations and helps to quantify the contributions of the respective boundary surfaces to the hemispheric LMS mass changes. The figure compares LMS mass changes for an LMS where all boundary surfaces evolve over time (as before, Fig. 12) with an LMS with only one boundary surface evolving over time ("floating"), while the other two are fixed (here, the first year of the time series is repeated).

ERA-Interim, MERRA-2, JRA-55 and JRA-3Q agree remarkably well on the mass decrease for the LMS defined between the lapse rate tropopause and 380 K (Fig. 14a–f). In ERA-Interim and MERRA-2, the dynamical upper LMS boundaries defined with respect to the tropical tropopause have the same effect as in ERA5: they partly compensate for the tropopause rise. On the other hand, in JRA-55 and JRA-3Q, the dynamical boundary surfaces add to the LMS mass decline in the NH. This contrasting behavior can be attributed to the differing temperature trends at the tropical tropopause across the reanalyses. Such differing (potential) temperature trends are visible not only at the tropical lapse rate tropopause and the cold point (Figs. 3, 10d and e), but also at pressure surfaces like 100 hPa (Fig. 4). Thus, the differences in the LMS mass trends between the JRA data sets and the other reanalyses are instead rooted in the reanalysis data sets themselves rather than in the analysis methods used in this study.

In Fig. 12c, the ERA5 LMS mass with respect to the SH lapse rate tropopause stands out with a significant LMS mass increase, regardless of the choice of the upper boundary. This is due to the increasing pressure trend in the SH extratropical lapse rate tropopause (Fig. 2a). Moreover, the intersection of the SH lapse rate tropopause with 350 K, which serves as the lateral LMS boundary, shows a small equatorward tendency (Fig. 11a). An interesting example is the respective LMS mass trends between 40–70° S (Fig. 12c). Since the ERA5 lapse rate tropopause change is close to zero between 40–70° S (Fig. 2a), the greater mass change for the SH LMS bounded with PPT10mean and PPTcp10mean compared to 380 K highlights the impact of the upper-boundary surface, which is confirmed again in Fig. 13b. In the SH, the mean LMS mass trends differ more strongly between the reanalyses than in the NH (Fig. 14g–l), especially for the LMS bounded by lrtp-380 K and lrtp-PPT10mean. Nevertheless, all reanalyses, except JRA-3Q, suggest increasing LMS mass in the SH. In general, the LMS mass trends reflect the respective lapse rate tropopause trends suggested by the reanalyses (Fig. 3). Like in the NH, the use of the dynamical upper boundaries (PT10mean and PTcp10mean) has a positive effect on the LMS mass trends in ERA5, ERA-Interim and MERRA-2, whereas the opposite applies for JRA-55 and JRA-3Q.

4 Conclusions

In this study, we analyzed long-term trends in the thermodynamic structure of the lowermost stratosphere based on reanalysis data for the period 1979–2019. We compare results for five modern reanalyses: ERA5, ERA-Interim, MERRA-2, JRA-55 and JRA-3Q. Our DLM trend analysis shows that the zonal mean NH mid-latitude tropopause exhibits a negative pressure trend of about −1 hPa per decade, consistent with increasing height trends between 1998–2019. Although the tropopause trends lack strong statistical significance, they

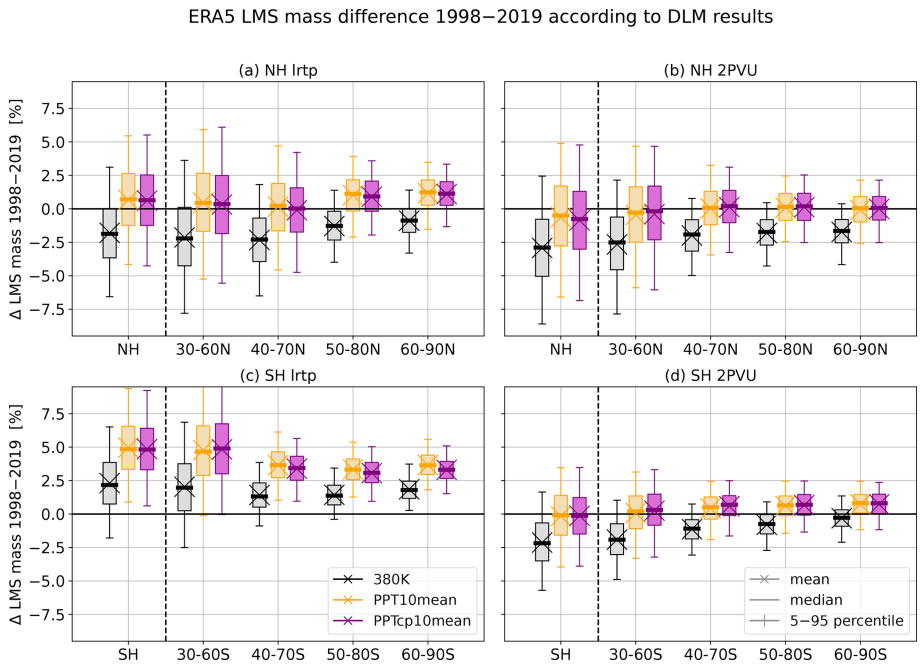

Figure 12. LMS mass change between 1998–2019 as estimated by the DLM from ERA5 data. The DLM trend state differences are presented as box-and-whisker plots. The LMS mass has been analyzed for different latitude bins (x axis) for both hemispheres **(a, b, c, d)**. The dashed vertical line separates the hemispheric trends from individual latitude bins. Moreover, different boundary surfaces have been compared. Panels **(a)** and **(c)** show the results for the LMS defined with the lapse rate tropopause as the lower boundary. In panels **(b)** and **(d)**, the 2 PVU tropopause serves as the lower LMS edge. The results for the different upper-boundary surfaces can be distinguished by the color of the box-and-whisker plots (380 K – black, PPT10mean – yellow, PPTcp10mean – purple).

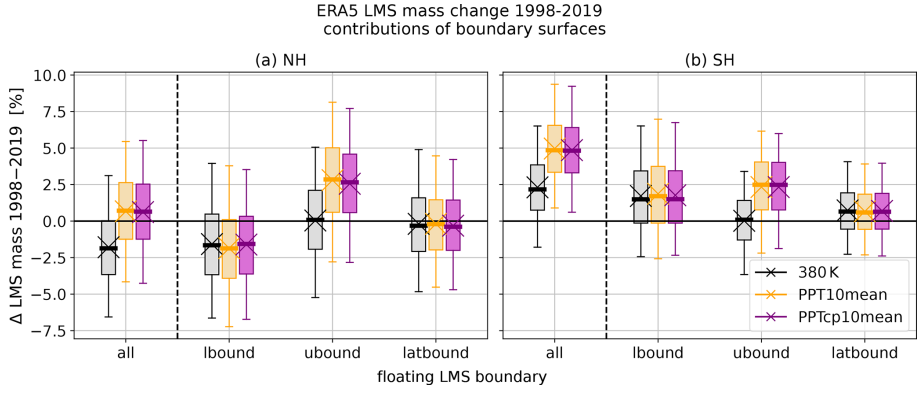

Figure 13. Similar to Fig. 12 but for hemispheric LMS mass difference if only one LMS boundary is allowed to evolve over time (floating), while the other two remain fixed, i.e., the year 1979 repeated. The respective boundaries are the lower boundary (lbound, here the lapse rate tropopause), the upper boundary (ubound, 380 K (black), PPT10mean (orange) or PTcp10mean (purple)) and the lateral boundary (latbound). For comparison, the LMS mass change between 1998–2019 for all boundary surfaces evolving over time is presented to the left of the dashed vertical line (same as in Fig. 12a and c).

are very robust across the reanalysis data sets and in line with observations (e.g., Xian and Homeyer, 2019; Meng et al., 2021). In the tropics and subtropics, the ERA5 lapse rate tropopause and the cold point show a statistically significant upward trend between 1979–2019, evident in pressure and geopotential height. The pressure trend amounts to about −0.5 hPa per decade at the tropical lapse rate tropopause and −0.7 hPa per decade at the cold point. These tropopause trends agree well with trends reported in other studies of reanalysis data (e.g., Wilcox et al., 2012; Xian and Homeyer, 2019) and observations (e.g., Meng et al., 2021). While all reanalyses examined in this study agree on decreasing tropopause pressure in the tropics, temperature trends in the TTL region are less consistent between the data sets.

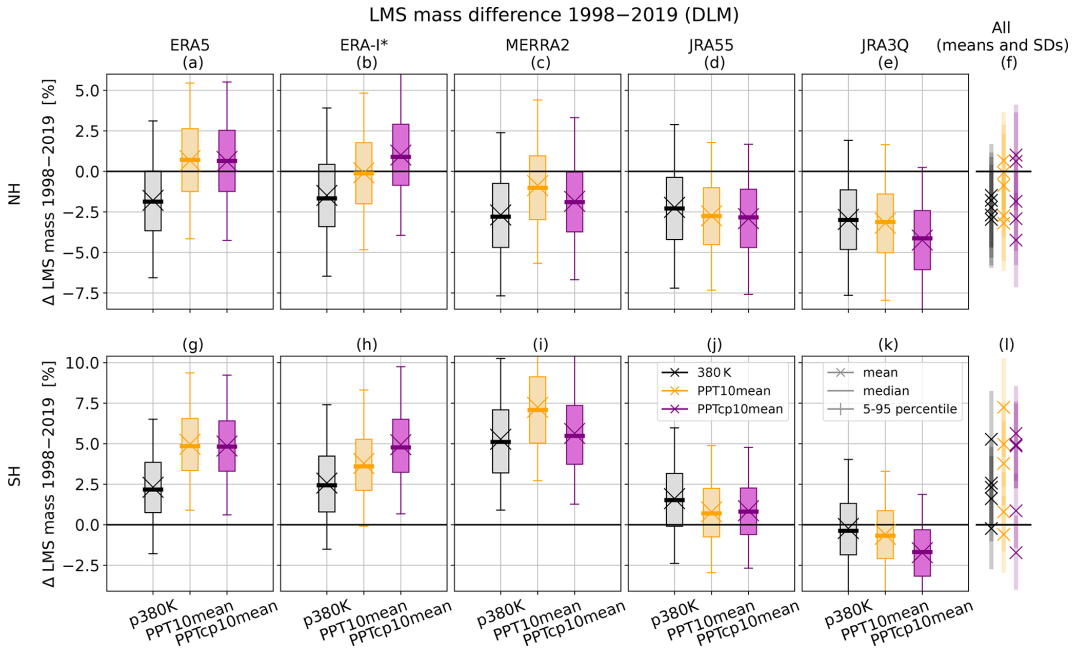

Figure 14. Similar to Fig. 12 but for LMS mass difference between 1998–2019 for different reanalyses (columns) on both hemispheres (rows). For better comparison, the mean trends (crosses) for all reanalyses are plotted again to the right of the figure **(f, l)**, together with their associated standard deviation (transparent lines). The lapse rate tropopause defines the lower LMS boundary. * ERA-Interim time series ends in 2018.

For ERA5, we find that potential temperatures at the tropical tropopause increase significantly, consistent with results from ERA-Interim and MERRA-2. JRA-55 and JRA-3Q, on the other hand, suggest the opposite tendency. The tendency of the SH tropopause in this study is less clear. In ERA5, the SH lapse rate tropopause shows a downward trend, accompanied by pressure trends ranging between 0 and +2 hPa per decade, whereas the 2 PVU surface rises at a mean rate of −1 hPa per decade. A positive pressure trend in the SH extratropical lapse rate tropopause is also evident in MERRA-2, JRA-55 and ERA-Interim and agrees with the trends found by Xian and Homeyer (2019) for the JRA-55, MERRA-2 and CFSR reanalyses. However, this positive pressure trend in the SH extratropical lapse rate tropopause seems to contradict the results reported for ERA-Interim in the same study and by Wilcox et al. (2012). Interestingly, our non-linear DLM trend analysis of the time series 1979–2019 reveals a trend reversal of the lapse rate tropopause around the year 2000. Accordingly, our results suggest decreasing pressure of the SH mid-latitude lapse rate tropopause before the year 2000 and increasing pressure thereafter. This could be consistent with expected effects of ozone recovery and an accelerating BDC on tropopause height in the SH (Birner, 2010b). An acceleration of the BDC in the SH after around the year 2000 has also been estimated from the age of air and long-lived trace gas measurements (Strahan et al., 2020; Ploeger and Garny, 2022).

The lateral positions of the intersections between the NH tropopause and isentropes between 330–370 K show a poleward shift after 1998, consistent across all reanalyses. The poleward tendency of the intersections can be associated with a widening of the tropics in the NH, which has been reported in many studies (e.g., Seidel and Randel, 2007; Meng et al., 2021; Wilcox et al., 2012; Grise et al., 2019; Staten et al., 2018). In the SH, the lateral trends in the intersections between the lapse rate tropopause and 350 K are directed equatorward, while 330 and 370 K show a poleward tendency, even though not all reanalyses agree in this case. The different magnitude of the lateral trends with respect to the potential temperature on both hemispheres suggests a steepening of the subtropical tropopause. A similar shape of lateral tropopause trends with respect to potential temperature has been found by Turhal et al. (2024) for the PV-gradient tropopause. Such a steepening of the subtropical tropopause, including the tropopause break, can be associated with an intensification of the SH subtropical jet (Manney and Hegglin, 2018; Maher et al., 2020) and could be linked to a strengthening of the BDC (Birner, 2010b).

Since the NH tropopause is rising and expanding toward the poles, the mass of the lowermost stratosphere (LMS) can be expected to decrease if the upper boundary is fixed. This expectation is confirmed by the robust mass decline in the northern hemispheric LMS bounded by the 380 K isentrope, which amounts to 2 %–3 % between 1998–2019, according to this study. However, as the upper LMS

boundary is properly defined by the tropical tropopause, which is also rising, the negative LMS mass trend is significantly reduced or even disappears when this dynamic upper boundary is used in the calculation. This is at least the case for ERA5, ERA-Interim and MERRA-2. JRA-55 and JRA-3Q show opposite temperature trends at the tropical tropopause. This by itself is an important finding, since TTL temperatures are a critical variable, not only impacting LMS mass, but also confining lower-stratospheric water vapor (e.g., Randel et al., 2004) and influencing stratospheric dynamics (e.g., Charlesworth et al., 2023). Why the reanalyses show the aforementioned discrepancies is beyond the scope of this study but should be investigated further. Indications of this can be found in SPARC (2022) and Fujiwara et al. (2024), suggesting relationships between differences in tropical lower-stratospheric temperature and radiative heating, related to ozone concentrations, among other factors.

Due to the downward trend in the SH lapse rate tropopause, evident in all reanalyses except JRA-3Q, which is accompanied by increasing pressure, the LMS mass in the SH is found to have increased by 1 %–7 % between 1998–2019. The different upper-boundary surfaces have the same effect on the LMS mass in the SH as in the NH: adding to the mass increase in ERA5, ERA-Interim and MERRA-2 but reducing it in JRA-55 and JRA-3Q. In general, the vertical boundaries dominate LMS mass changes. However, tropical width changes can have a considerable impact on LMS mass due to the area decrease from low to high latitudes.

LMS mass changes are important to consider because the LMS mass makes up a considerable amount of the stratospheric column, in our case approximately 20 %, and therefore contains a substantial fraction of, for example, column ozone. Since the interannual ozone variability in the LMS is mainly controlled by dynamics (e.g., Chipperfield et al., 2018), ozone changes are expected to be directly related to LMS mass changes. LMS ozone changes have important implications for not only the radiative budget in the lower stratosphere but also atmospheric chemistry and the UV radiation reaching the surface (e.g., Forster and Shine, 1997; Hegglin and Shepherd, 2009).

Appendix A

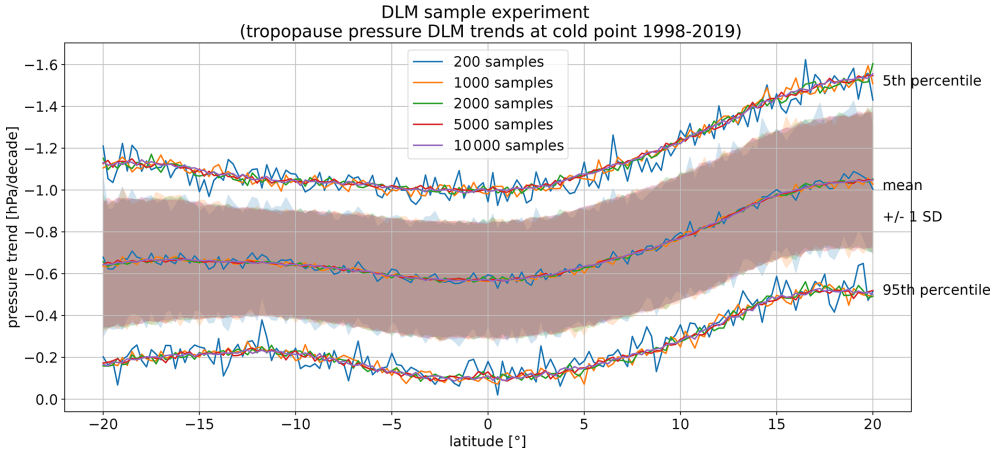

Figure A1. Illustration of the sensitivity of DLM trend estimates to the number of DLM samples using the example of cold-point pressure trends between 1998–2019.

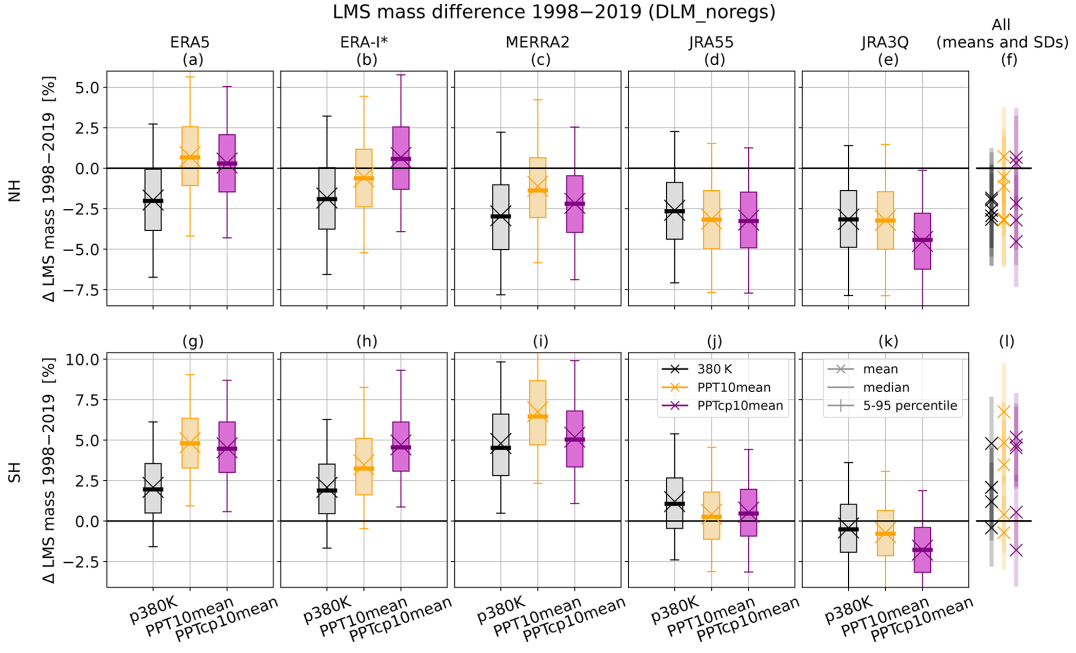

Figure A2. Same as Fig. 14 but for DLM analysis without regressors.

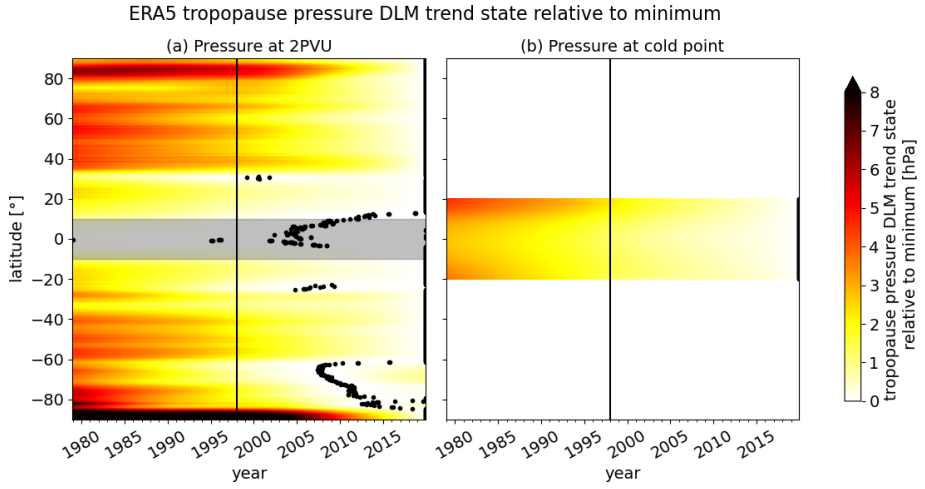

Figure A3. Same as Fig. 5 but for the ERA5 2 PVU dynamic tropopause **(a)** and the cold point **(b)**. Note that since the 2 PVU isosurface is capped at a fixed pressure of 89 hPa in the inner tropics, the respective pressure trends are not meaningful (gray shading).

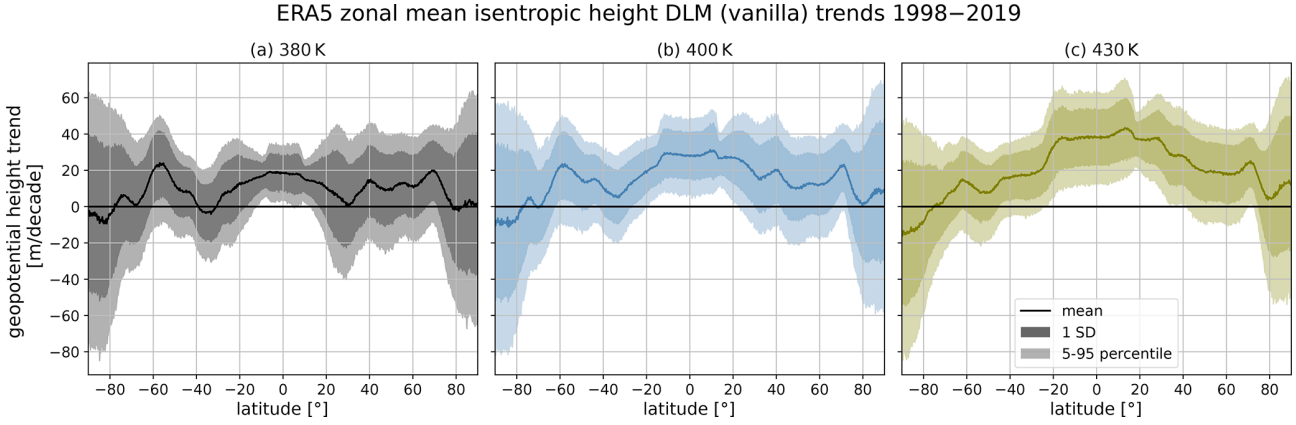

Figure A4. Same as Fig. 6a–c but for geopotential height trends.

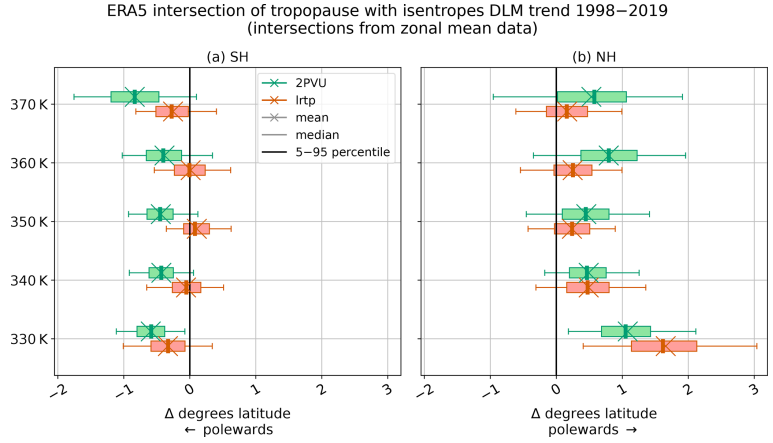

Figure A5. Same as Fig. 11 but for the intersections between isentropes with the lapse rate tropopause (red) and the 2 PVU dynamic tropopause in ERA5.

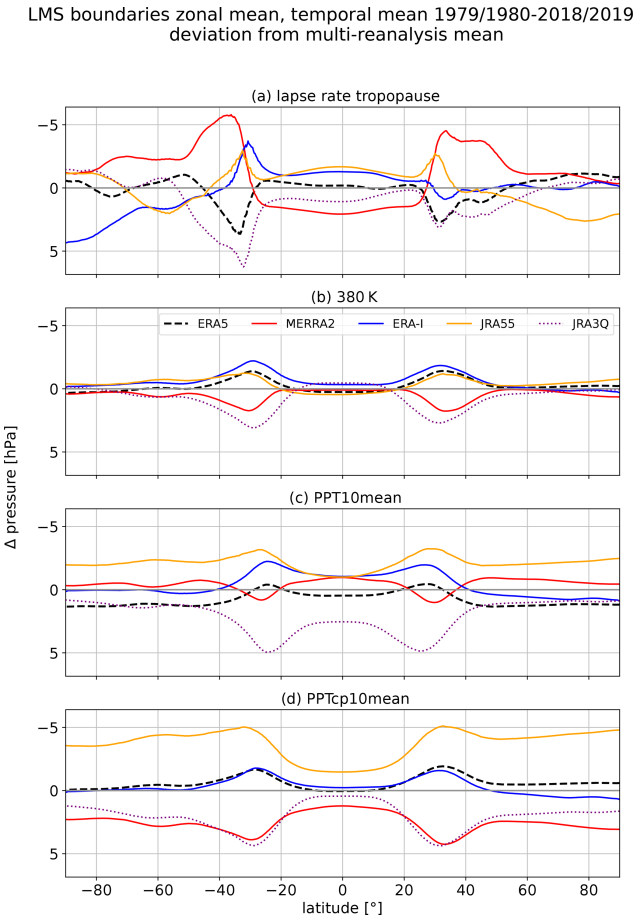

Figure A6. Illustration of the differences in the location of the LMS boundary surfaces, i.e., the lapse rate tropopause **(a)**, 380 K **(b)**, PPT10mean **(c)** and PPTcp10mean **(d)** across the reanalyses (ERA5, black, dashed; MERRA-2, red, solid; ERA-Interim, blue, solid; JRA-55, orange, solid; JRA-3Q, purple, dotted). Shown are the deviations from the multi-reanalysis mean in hectopascals. Note that the *y* axis is inverted because pressure decreases with altitude. ERA5, JRA-55 and JRA-3Q span the time period 1979–2019; MERRA-2 spans the time period 1980–2019; and ERA-Interim spans the time period 1979–2018.

Table A1. Mean LMS mass and associated standard deviation in 10^{17} kg for different LMS definitions and reanalysis data sets.

LMS definition	Reanalysis	NH	SH
lrtp-380K	ERA5	0.55 ± 0.20	0.57 ± 0.10
	MERRA-2	0.50 ± 0.20	0.51 ± 0.11
	ERA-Interim	0.54 ± 0.20	0.57 ± 0.11
	JRA-55	0.53 ± 0.19	0.56 ± 0.10
	JRA-3Q	0.54 ± 0.19	0.57 ± 0.10
lrtp-PPT10mean	ERA5	0.49 ± 0.20	0.50 ± 0.08
	MERRA-2	0.46 ± 0.19	0.46 ± 0.10
	ERA-Interim	0.49 ± 0.20	0.51 ± 0.09
	JRA-55	0.49 ± 0.19	0.51 ± 0.09
	JRA-3Q	0.49 ± 0.18	0.51 ± 0.08
lrtp-PPTcp10mean	ERA5	0.56 ± 0.22	0.58 ± 0.09
	MERRA-2	0.49 ± 0.21	0.50 ± 0.10
	ERA-Interim	0.55 ± 0.22	0.57 ± 0.10
	JRA-55	0.56 ± 0.21	0.58 ± 0.09
	JRA-3Q	0.54 ± 0.20	0.57 ± 0.08

Code and data availability. ERA5 and ERA-Interim reanalysis data are available from the European Centre for Medium-range Weather Forecasts (https://doi.org/10.24381/cds.143582cf, Hersbach et al., 2017; https://doi.org/10.24381/cds.f2f5241d, Dee et al., 2011a). The MERRA-2 data set is provided by the Global Modeling And Assimilation Office and Pawson (2015) (https://doi.org/10.5067/2E096JV59PK7) of the National Aeronautics and Space Administration (NASA). The JRA-55 reanalysis data are available at https://doi.org/10.5065/D60G3H5B (Japan Meteorological Agency/Japan, 2013), and the JRA-3Q data set is available at https://doi.org/10.5065/CW01-2282 (Japan Meteorological Agency/Japan, 2024). The DLM code (dlmmc) is publicly available at https://doi.org/10.5281/zenodo.2660704 (Alsing and Smith, 2019). The code for LMS mass calculation and trend analysis, including the respective LMS boundary surfaces in all reanalyses, is available on Zenodo at https://doi.org/10.5281/zenodo.13890231 (Weyland, 2024).

Author contributions. FW performed the analyses and wrote the first draft of the paper. PH and DK initiated the project and conceptualized the core research goals. FP and TB contributed valuable ideas. KT provided the PV-gradient tropopause data. All authors contributed to the interpretation of the results and improvement of the paper.

Competing interests. The contact author has declared that none of the authors has any competing interests.

Disclaimer. Publisher's note: Copernicus Publications remains neutral with regard to jurisdictional claims made in the text, published maps, institutional affiliations, or any other geographical representation in this paper. While Copernicus Publications makes every effort to include appropriate place names, the final responsibility lies with the authors.

Special issue statement. This article is part of the special issue "The SPARC Reanalysis Intercomparison Project (S-RIP) Phase 2 (ACP/WCD inter-journal SI)". It is not associated with a conference.

Acknowledgements. We would like to thank the Dres. Göbel Klima-Stiftung for their financial support, which Franziska Weyland was able to benefit from as part of a Deutschlandstipendium during her master's program.

Financial support. This research has been supported by the Deutsche Forschungsgemeinschaft (TPChange grant, The Tropopause Region in a Changing Atmosphere, DFG TRR 301, project ID 428312742). The project has also been supported as part of HALO SPP 1294 under grant no. HO-4225/19-1.

Review statement. This paper was edited by Petr Šácha and reviewed by Juan Antonio Añel and two anonymous referees.

References

Alsing, J.: dlmmc: Dynamical linear model regression for atmospheric time-series analysis, Journal of Open Source Software, 4, 1157, https://doi.org/10.21105/joss.01157, 2019.

Alsing, J., and Smith, A.: justinalsing/dlmmc: Second release (v1.1), Zenodo [code], https://doi.org/10.5281/zenodo.2660704, 2019.

Appenzeller, C., Holton, J. R., and Rosenlof, K. H.: Seasonal variation of mass transport across the tropopause, J. Geophys. Res.-Atmos., 101, 15071–15078, https://doi.org/10.1029/96JD00821, 1996.

Ball, W. T., Alsing, J., Mortlock, D. J., Rozanov, E. V., Tummon, F., and Haigh, J. D.: Reconciling differences in stratospheric ozone composites, Atmos. Chem. Phys., 17, 12269–12302, https://doi.org/10.5194/acp-17-12269-2017, 2017.

Ball, W. T., Alsing, J., Mortlock, D. J., Staehelin, J., Haigh, J. D., Peter, T., Tummon, F., Stübi, R., Stenke, A., Anderson, J., Bourassa, A., Davis, S. M., Degenstein, D., Frith, S., Froidevaux, L., Roth, C., Sofieva, V., Wang, R., Wild, J., Yu, P., Ziemke, J. R., and Rozanov, E. V.: Evidence for a continuous decline in lower stratospheric ozone offsetting ozone layer recovery, Atmos. Chem. Phys., 18, 1379–1394, https://doi.org/10.5194/acp-18-1379-2018, 2018.

Ball, W. T., Alsing, J., Staehelin, J., Davis, S. M., Froidevaux, L., and Peter, T.: Stratospheric ozone trends for 1985–2018: sensitivity to recent large variability, Atmos. Chem. Phys., 19, 12731–12748, https://doi.org/10.5194/acp-19-12731-2019, 2019.

Berthet, G., Esler, J. G., and Haynes, P. H.: A Lagrangian perspective of the tropopause and the ventilation of the lowermost stratosphere, J. Geophys. Res.-Atmos., 112, 2006JD008295, https://doi.org/10.1029/2006JD008295, 2007.

Bethan, S., Vaughan, G., and Reid, S. J.: A comparison of ozone and thermal tropopause heights and the impact of tropopause definition on quantifying the ozone content of the troposphere, Q. J. Roy. Meteor. Soc., 122, 929–944, https://doi.org/10.1002/qj.49712253207, 1996.

Birner, T.: Fine-scale structure of the extratropical tropopause region, J. Geophys. Res.-Atmos., 111, 2005JD006301, https://doi.org/10.1029/2005JD006301, 2006.

Birner, T.: Recent widening of the tropical belt from global tropopause statistics: Sensitivities, J. Geophys. Res.-Atmos., 115, 2010JD014664, https://doi.org/10.1029/2010JD014664, 2010a.

Birner, T.: Residual Circulation and Tropopause Structure, J. Atmos. Sci., 67, 2582–2600, https://doi.org/10.1175/2010JAS3287.1, 2010b.

Birner, T., Dörnbrack, A., and Schumann, U.: How sharp is the tropopause at midlatitudes?, Geophys. Res. Lett., 29, 45-1–45-4, https://doi.org/10.1029/2002GL015142, 2002.

Bognar, K., Tegtmeier, S., Bourassa, A., Roth, C., Warnock, T., Zawada, D., and Degenstein, D.: Stratospheric ozone trends for 1984–2021 in the SAGE II–OSIRIS–SAGE II-I/ISS composite dataset, Atmos. Chem. Phys., 22, 9553–9569, https://doi.org/10.5194/acp-22-9553-2022, 2022.

Boljka, L. and Birner, T.: Potential impact of tropopause sharpness on the structure and strength of the general circulation, npj Climate and Atmospheric Science, 5, 98, https://doi.org/10.1038/s41612-022-00319-6, 2022.

Butchart, N.: The Brewer-Dobson circulation, Rev. Geophys., 52, 157–184, https://doi.org/10.1002/2013RG000448, 2014.

Castanheira, J. M., Añel, J. A., Marques, C. A. F., Antuña, J. C., Liberato, M. L. R., de la Torre, L., and Gimeno, L.: Increase of upper troposphere/lower stratosphere wave baroclinicity during the second half of the 20th century, Atmos. Chem. Phys., 9, 9143–9153, https://doi.org/10.5194/acp-9-9143-2009, 2009.

Charlesworth, E., Plöger, F., Birner, T., Baikhadzhaev, R., Abalos, M., Abraham, N. L., Akiyoshi, H., Bekki, S., Dennison, F., Jöckel, P., Keeble, J., Kinnison, D., Morgenstern, O., Plummer, D., Rozanov, E., Strode, S., Zeng, G., Egorova, T., and Riese, M.: Stratospheric water vapor affecting atmospheric circulation, Nat. Commun., 14, 3925, https://doi.org/10.1038/s41467-023-39559-2, 2023.

Chipperfield, M. P., Dhomse, S., Hossaini, R., Feng, W., Santee, M. L., Weber, M., Burrows, J. P., Wild, J. D., Loyola, D., and Coldewey-Egbers, M.: On the Cause of Recent Variations in Lower Stratospheric Ozone, Geophys. Res. Lett., 45, 5718–5726, https://doi.org/10.1029/2018GL078071, 2018.

Dee, D., Uppala, S., Simmons, A., Berrisford, P., Poli, P., Kobayashi, S., Andrae, U., Balmaseda, M., Balsamo, G., Bauer, P., Bechtold, P., Beljaars, A., van de Berg, L., Bidlot, J., Bormann, N., Delsol, C., Dragani, R., Fuentes, M., Geer, A., Haimberger, L., Healy, S., Hersbach, H., Hólm, E., Isaksen, L., Kållberg, P., Köhler, M., Matricardi, M., McNally, A., Monge-Sanz, B., Morcrette, J., Park, B., Peubey, C., de Rosnay, P., Tavolato, C., Thépaut, J., and Vitart, F.: ERA-Interim global atmospheric reanalysis, Copernicus Climate Change Service (C3S) Climate Data Store (CDS) [data set], https://doi.org/10.24381/cds.f2f5241d, 2011a.

Dee, D. P., Uppala, S. M., Simmons, A. J., Berrisford, P., Poli, P., Kobayashi, S., Andrae, U., Balmaseda, M. A., Balsamo, G., Bauer, P., Bechtold, P., Beljaars, A. C. M., Van De Berg, L., Bidlot, J., Bormann, N., Delsol, C., Dragani, R., Fuentes, M., Geer, A. J., Haimberger, L., Healy, S. B., Hersbach, H., Hólm, E. V., Isaksen, L., Kållberg, P., Köhler, M., Matricardi, M., McNally, A. P., Monge-Sanz, B. M., Morcrette, J., Park, B., Peubey, C., De Rosnay, P., Tavolato, C., Thépaut, J., and Vitart, F.: The ERA-Interim reanalysis: configuration and performance of the data assimilation system, Q. J. Roy. Meteor. Soc., 137, 553–597, https://doi.org/10.1002/qj.828, 2011b.

ECMWF: IFS Documentation CY41R2 – Part VI: Technical and Computational Procedures, https://doi.org/10.21957/5RWD87QEW, 2016.

Eichinger, R. and Šácha, P.: Overestimated acceleration of the advective Brewer–Dobson circulation due to strato-

spheric cooling, Q. J. Roy. Meteor. Soc., 146, 3850–3864, https://doi.org/10.1002/qj.3876, 2020.

Fischer, H., Wienhold, F. G., Hoor, P., Bujok, O., Schiller, C., Siegmund, P., Ambaum, M., Scheeren, H. A., and Lelieveld, J.: Tracer correlations in the northern high latitude lowermost stratosphere: Influence of cross-tropopause mass exchange, Geophys. Res. Lett., 27, 97–100, https://doi.org/10.1029/1999GL010879, 2000.

de F. Forster, P. M. and Shine, K. P.: Radiative forcing and temperature trends from stratospheric ozone changes, J. Geophys. Res.-Atmos., 102, 10841–10855, https://doi.org/10.1029/96JD03510, 1997.

Forster, P. M. D. F. and Shine, K. P.: Assessing the climate impact of trends in stratospheric water vapor, Geophys. Res. Lett., 29, 1086, https://doi.org/10.1029/2001GL013909, 2002.

Fu, Q., Solomon, S., Pahlavan, H. A., and Lin, P.: Observed changes in Brewer–Dobson circulation for 1980–2018, Environ. Res. Lett., 14, 114026, https://doi.org/10.1088/1748-9326/ab4de7, 2019.

FU-Berlin: The Quasi-Biennial oscillation (QBO) Data Serie, https://www.geo.fu-berlin.de/met/ag/strat/produkte/qbo/qbo.dat, last access: 11 July 2023.

Fujiwara, M., Martineau, P., Wright, J. S., Abalos, M., Šácha, P., Kawatani, Y., Davis, S. M., Birner, T., and Monge-Sanz, B. M.: Climatology of the terms and variables of transformed Eulerian-mean (TEM) equations from multiple reanalyses: MERRA-2, JRA-55, ERA-Interim, and CFSR, Atmos. Chem. Phys., 24, 7873–7898, https://doi.org/10.5194/acp-24-7873-2024, 2024.

Gelaro, R., McCarty, W., Suárez, M. J., Todling, R., Molod, A., Takacs, L., Randles, C. A., Darmenov, A., Bosilovich, M. G., Reichle, R., Wargan, K., Coy, L., Cullather, R., Draper, C., Akella, S., Buchard, V., Conaty, A., Da Silva, A. M., Gu, W., Kim, G.-K., Koster, R., Lucchesi, R., Merkova, D., Nielsen, J. E., Partyka, G., Pawson, S., Putman, W., Rienecker, M., Schubert, S. D., Sienkiewicz, M., and Zhao, B.: The Modern-Era Retrospective Analysis for Research and Applications, Version 2 (MERRA-2), J. Climate, 30, 5419–5454, https://doi.org/10.1175/JCLI-D-16-0758.1, 2017.

Gettelman, A. and Wang, T.: Structural diagnostics of the tropopause inversion layer and its evolution, J. Geophys. Res.-Atmos., 120, 46–62, https://doi.org/10.1002/2014JD021846, 2015.

Gettelman, A., Hoor, P., Pan, L. L., Randel, W. J., Hegglin, M. I., and Birner, T.: The Extratropical Upper Troposphere and Lower Stratosphere, Rev. Geophys., 49, RG3003, https://doi.org/10.1029/2011RG000355, 2011.

Global Modeling And Assimilation Office and Pawson, S.: MERRA-2 instM_3d_asm_Np: 3d,Monthly mean,Instantaneous,Pressure-Level,Assimilation,Assimilated Meteorological Fields V5.12.4, GES DISC [data set], https://doi.org/10.5067/2E096JV59PK7, 2015.

Grise, K. M., Davis, S. M., Simpson, I. R., Waugh, D. W., Fu, Q., Allen, R. J., Rosenlof, K. H., Ummenhofer, C. C., Karnauskas, K. B., Maycock, A. C., Quan, X.-W., Birner, T., and Staten, P. W.: Recent Tropical Expansion: Natural Variability or Forced Response?, J. Climate, 32, 1551–1571, https://doi.org/10.1175/JCLI-D-18-0444.1, 2019.

Hegglin, M. I. and Shepherd, T. G.: Large climate-induced changes in ultraviolet index and stratosphere-to-troposphere ozone flux, Nat. Geosci., 2, 687–691, https://doi.org/10.1038/ngeo604, 2009.

Hegglin, M. I., Gettelman, A., Hoor, P., Krichevsky, R., Manney, G. L., Pan, L. L., Son, S.-W., Stiller, G., Tilmes, S., Walker, K. A., Eyring, V., Shepherd, T. G., Waugh, D., Akiyoshi, H., Añel, J. A., Austin, J., Baumgaertner, A., Bekki, S., Braesicke, P., Brühl, C., Butchart, N., Chipperfield, M., Dameris, M., Dhomse, S., Frith, S., Garny, H., Hardiman, S. C., Jöckel, P., Kinnison, D. E., Lamarque, J. F., Mancini, E., Michou, M., Morgenstern, O., Nakamura, T., Olivié, D., Pawson, S., Pitari, G., Plummer, D. A., Pyle, J. A., Rozanov, E., Scinocca, J. F., Shibata, K., Smale, D., Teyssèdre, H., Tian, W., and Yamashita, Y.: Multimodel assessment of the upper troposphere and lower stratosphere: Extratropics, J. Geophys. Res., 115, D00M09, https://doi.org/10.1029/2010JD013884, 2010.

Hersbach, H., Bell, B., Berrisford, P., Hirahara, S., Horányi, A., Muñoz-Sabater, J., Nicolas, J., Peubey, C., Radu, R., Schepers, D., Simmons, A., Soci, C., Abdalla, S., Abellan, X., Balsamo, G., Bechtold, P., Biavati, G., Bidlot, J., Bonavita, M., De Chiara, G., Dahlgren, P., Dee, D., Diamantakis, M., Dragani, R., Flemming, J., Forbes, R., Fuentes, M., Geer, A., Haimberger, L., Healy, S., Hogan, R., Hólm, E., Janisková, M., Keeley, S., Laloyaux, P., Lopez, P., Lupu, C., Radnoti, G., de Rosnay, P., Rozum, I., Vamborg, F., Villaume, S., and Thépaut, J.-N.: Complete ERA5 from 1940: Fifth generation of ECMWF atmospheric reanalyses of the global climate, Copernicus Climate Change Service (C3S) Data Store (CDS) [data set], https://doi.org/10.24381/cds.143582cf, 2017.

Hersbach, H., Bell, B., Berrisford, P., Hirahara, S., Horányi, A., Muñoz-Sabater, J., Nicolas, J., Peubey, C., Radu, R., Schepers, D., Simmons, A., Soci, C., Abdalla, S., Abellan, X., Balsamo, G., Bechtold, P., Biavati, G., Bidlot, J., Bonavita, M., Chiara, G., Dahlgren, P., Dee, D., Diamantakis, M., Dragani, R., Flemming, J., Forbes, R., Fuentes, M., Geer, A., Haimberger, L., Healy, S., Hogan, R. J., Hólm, E., Janisková, M., Keeley, S., Laloyaux, P., Lopez, P., Lupu, C., Radnoti, G., Rosnay, P., Rozum, I., Vamborg, F., Villaume, S., and Thépaut, J.: The ERA5 global reanalysis, Q. J. Roy. Meteor. Soc., 146, 999–2049, https://doi.org/10.1002/qj.3803, 2020.

Hoerling, M. P., Schaack, T. D., and Lenzen, A. J.: Global objective tropopause analysis, Mon. Weather Rev., 119, 1816–1831, https://doi.org/10.1175/1520-0493(1991)119<1816:gota>2.0.co;2, 1991.

Holton, J. R., Haynes, P. H., McIntyre, M. E., Douglass, A. R., Rood, R. B., and Pfister, L.: Stratosphere-troposphere exchange, Rev. Geophys., 33, 403, https://doi.org/10.1029/95RG02097, 1995.

Hoor, P., Fischer, H., Lange, L., Lelieveld, J., and Brunner, D.: Seasonal variations of a mixing layer in the lowermost stratosphere as identified by the CO--O_3 correlation from in situ measurements, J. Geophys. Res.-Atmos., 107, 4044, https://doi.org/10.1029/2000JD000289, 2002.

Hoor, P., Gurk, C., Brunner, D., Hegglin, M. I., Wernli, H., and Fischer, H.: Seasonality and extent of extratropical TST derived from in-situ CO measurements during SPURT, Atmos. Chem. Phys., 4, 1427–1442, https://doi.org/10.5194/acp-4-1427-2004, 2004.

Hoskins, B. J.: Towards a PV-theta view of the general circulation, Tellus A, 43, 27–35, https://doi.org/10.1034/j.1600-0870.1991.t01-3-00005.x, 1991.

IPCC, Calvin, K., Dasgupta, D., Krinner, G., Mukherji, A., Thorne, P. W., Trisos, C., Romero, J., Aldunce, P., Barrett, K., Blanco, G., Cheung, W. W., Connors, S., Denton, F., Diongue-Niang, A., Dodman, D., Garschagen, M., Geden, O., Hayward, B., Jones, C., Jotzo, F., Krug, T., Lasco, R., Lee, Y.-Y., Masson-Delmotte, V., Meinshausen, M., Mintenbeck, K., Mokssit, A., Otto, F. E., Pathak, M., Pirani, A., Poloczanska, E., Pörtner, H.-O., Revi, A., Roberts, D. C., Roy, J., Ruane, A. C., Skea, J., Shukla, P. R., Slade, R., Slangen, A., Sokona, Y., Sörensson, A. A., Tignor, M., Van Vuuren, D., Wei, Y.-M., Winkler, H., Zhai, P., Zommers, Z., Hourcade, J.-C., Johnson, F. X., Pachauri, S., Simpson, N. P., Singh, C., Thomas, A., Totin, E., Arias, P., Bustamante, M., Elgizouli, I., Flato, G., Howden, M., Méndez-Vallejo, C., Pereira, J. J., Pichs-Madruga, R., Rose, S. K., Saheb, Y., Sánchez Rodríguez, R., Ürge Vorsatz, D., Xiao, C., Yassaa, N., Alegría, A., Armour, K., Bednar-Friedl, B., Blok, K., Cissé, G., Dentener, F., Eriksen, S., Fischer, E., Garner, G., Guivarch, C., Haasnoot, M., Hansen, G., Hauser, M., Hawkins, E., Hermans, T., Kopp, R., Leprince-Ringuet, N., Lewis, J., Ley, D., Ludden, C., Niamir, L., Nicholls, Z., Some, S., Szopa, S., Trewin, B., Van Der Wijst, K.-I., Winter, G., Witting, M., Birt, A., Ha, M., Romero, J., Kim, J., Haites, E. F., Jung, Y., Stavins, R., Birt, A., Ha, M., Orendain, D. J. A., Ignon, L., Park, S., Park, Y., Reisinger, A., Cammaramo, D., Fischlin, A., Fuglestvedt, J. S., Hansen, G., Ludden, C., Masson-Delmotte, V., Matthews, J. R., Mintenbeck, K., Pirani, A., Poloczanska, E., Leprince-Ringuet, N., and Péan, C.: IPCC, 2023: Climate Change 2023: Synthesis Report. Contribution of Working Groups I, II and III to the Sixth Assessment Report of the Intergovernmental Panel on Climate Change [Core Writing Team, edited by: Lee, H. and Romero, J., IPCC, Geneva, Switzerland, Tech. rep., Intergovernmental Panel on Climate Change (IPCC), https://doi.org/10.59327/IPCC/AR6-9789291691647, 2023.

Japan Meteorological Agency/Japan: JRA-55: Japanese 55-year Reanalysis, Monthly Means and Variances, NCAR [data set], https://doi.org/10.5065/D60G3H5B, 2013.

Japan Meteorological Agency/Japan: Near real-time monthly mean Japanese Reanalysis for Three Quarters of a Century (JRA-3Q), NCAR [data set], https://doi.org/10.5065/CW01-2282, 2024.

JMA: Information Infrastructure Department, Japan Meteorological Agency, JRA-3Q Data Format – Model grid data, https://jra.kishou.go.jp/JRA-3Q/document/JRA-3Q_TL479_format_en.pdf, last access: 1 October 2024.

Kaluza, T., Kunkel, D., and Hoor, P.: On the occurrence of strong vertical wind shear in the tropopause region: a 10-year ERA5 northern hemispheric study, Weather Clim. Dynam., 2, 631–651, https://doi.org/10.5194/wcd-2-631-2021, 2021.

Karagodin-Doyennel, A., Rozanov, E., Sukhodolov, T., Egorova, T., Sedlacek, J., Ball, W., and Peter, T.: The historical ozone trends simulated with the SOCOLv4 and their comparison with observations and reanalyses, Atmos. Chem. Phys., 22, 15333–15350, https://doi.org/10.5194/acp-22-15333-2022, 2022.

Kobayashi, S., Ota, Y., Harada, Y., Ebita, A., Moriya, M., Onoda, H., Onogi, K., Kamahori, H., Kobayashi, C., Endo, H., Miyaoka, K., and Takahashi, K.: The JRA-55 Reanalysis: General Specifications and Basic Characteristics, J. Meteorol. Soc. Jpn., 93, 5–48, https://doi.org/10.2151/jmsj.2015-001, 2015.

Kosaka, Y., Kobayashi, S., Harada, Y., Kobayashi, C., Naoe, H., Yoshimoto, K., Harada, M., Goto, N., Chiba, J., Miyaoka, K., Sekiguchi, R., Deushi, M., Kamahori, H., Nakaegawa, T., Tanaka, T. Y., Tokuhiro, T., Sato, Y., Matsushita, Y., and Onogi, K.: The JRA-3Q Reanalysis, J. Meteorol. Soc. Jpn., 102, 49–109, https://doi.org/10.2151/jmsj.2024-004, 2024.

Kunkel, D., Hoor, P., Kaluza, T., Ungermann, J., Kluschat, B., Giez, A., Lachnitt, H.-C., Kaufmann, M., and Riese, M.: Evidence of small-scale quasi-isentropic mixing in ridges of extratropical baroclinic waves, Atmos. Chem. Phys., 19, 12607–12630, https://doi.org/10.5194/acp-19-12607-2019, 2019.

Kunz, A., Konopka, P., Müller, R., and Pan, L. L.: Dynamical tropopause based on isentropic potential vorticity gradients, J. Geophys. Res., 116, D01110, https://doi.org/10.1029/2010JD014343, 2011.

Laine, M., Latva-Pukkila, N., and Kyrölä, E.: Analysing time-varying trends in stratospheric ozone time series using the state space approach, Atmos. Chem. Phys., 14, 9707–9725, https://doi.org/10.5194/acp-14-9707-2014, 2014.

Lu, J., Deser, C., and Reichler, T.: Cause of the widening of the tropical belt since 1958, Geophys. Res. Lett., 36, 2008GL036076, https://doi.org/10.1029/2008GL036076, 2009.

Maher, P., Kelleher, M. E., Sansom, P. G., and Methven, J.: Is the subtropical jet shifting poleward?, Clim. Dynam., 54, 1741–1759, https://doi.org/10.1007/s00382-019-05084-6, 2020.

Manney, G. L. and Hegglin, M. I.: Seasonal and Regional Variations of Long-Term Changes in Upper-Tropospheric Jets from Reanalyses, J. Climate, 31, 423–448, https://doi.org/10.1175/JCLI-D-17-0303.1, 2018.

Manney, G. L., Hegglin, M. I., Daffer, W. H., Santee, M. L., Ray, E. A., Pawson, S., Schwartz, M. J., Boone, C. D., Froidevaux, L., Livesey, N. J., Read, W. G., and Walker, K. A.: Jet characterization in the upper troposphere/lower stratosphere (UTLS): applications to climatology and transport studies, Atmos. Chem. Phys., 11, 6115–6137, https://doi.org/10.5194/acp-11-6115-2011, 2011.

Meng, L., Liu, J., Tarasick, D. W., Randel, W. J., Steiner, A. K., Wilhelmsen, H., Wang, L., and Haimberger, L.: Continuous rise of the tropopause in the Northern Hemisphere over 1980–2020, Science Advances, 7, eabi8065, https://doi.org/10.1126/sciadv.abi8065, 2021.

Minganti, D., Chabrillat, S., Errera, Q., Prignon, M., Kinnison, D. E., Garcia, R. R., Abalos, M., Alsing, J., Schneider, M., Smale, D., Jones, N., and Mahieu, E.: Evaluation of the N_2O Rate of Change to Understand the Stratospheric Brewer-Dobson Circulation in a Chemistry-Climate Model, J. Geophys. Res.-Atmos., 127, e2021JD036390, https://doi.org/10.1029/2021JD036390, 2022.

NOAA: Multivariate ENSO Index Version 2 (MEI.v2), https://psl.noaa.gov/enso/mei/, last access: 11 July 2023.

Oberländer-Hayn, S., Gerber, E. P., Abalichin, J., Akiyoshi, H., Kerschbaumer, A., Kubin, A., Kunze, M., Langematz, U., Meul, S., Michou, M., Morgenstern, O., and Oman, L. D.: Is the Brewer-Dobson circulation increasing or moving upward?, Geophys. Res. Lett., 43, 1772–1779, https://doi.org/10.1002/2015GL067545, 2016.

Olsen, M. A., Douglass, A. R., and Kaplan, T. B.: Variability of extratropical ozone stratosphere–troposphere exchange using microwave limb sounder observations, J. Geophys. Res.-Atmos., 118, 1090–1099, https://doi.org/10.1029/2012JD018465, 2013.

Pan, L. L., Randel, W. J., Gary, B. L., Mahoney, M. J., and Hintsa, E. J.: Definitions and sharpness of the extratropical tropopause: A trace gas perspective, J. Geophys. Res.-Atmos., 109, 2004JD004982, https://doi.org/10.1029/2004JD004982, 2004.

Pisoft, P., Šácha, P., Polvani, L. M., Añel, J. A., De La Torre, L., Eichinger, R., Foelsche, U., Huszar, P., Jacobi, C., Karlicky, J., Kuchar, A., Miksovsky, J., Zak, M., and Rieder, H. E.: Stratospheric contraction caused by increasing greenhouse gases, Environ. Res. Lett., 16, 064038, https://doi.org/10.1088/1748-9326/abfe2b, 2021.

Ploeger, F. and Garny, H.: Hemispheric asymmetries in recent changes in the stratospheric circulation, Atmos. Chem. Phys., 22, 5559–5576, https://doi.org/10.5194/acp-22-5559-2022, 2022.

Ramaswamy, V., Chanin, M., Angell, J., Barnett, J., Gaffen, D., Gelman, M., Keckhut, P., Koshelkov, Y., Labitzke, K., Lin, J. R., O'Neill, A., Nash, J., Randel, W., Rood, R., Shine, K., Shiotani, M., and Swinbank, R.: Stratospheric temperature trends: Observations and model simulations, Rev. Geophys., 39, 71–122, https://doi.org/10.1029/1999RG000065, 2001.

Randel, W. J., Wu, F., Oltmans, S. J., Rosenlof, K., and Nedoluha, G. E.: Interannual Changes of Stratospheric Water Vapor and Correlations with Tropical Tropopause Temperatures, J. Atmos. Sci., 61, 2133–2148, https://doi.org/10.1175/1520-0469(2004)061<2133:ICOSWV>2.0.CO;2, 2004.

Randel, W. J., Wu, F., and Forster, P.: The Extratropical Tropopause Inversion Layer: Global Observations with GPS Data, and a Radiative Forcing Mechanism, J. Atmos. Sci., 64, 4489–4496, https://doi.org/10.1175/2007JAS2412.1, 2007.

Reichler, T., Dameris, M., and Sausen, R.: Determining the tropopause height from gridded data, Geophys. Res. Lett., 30, 2003GL018240, https://doi.org/10.1029/2003GL018240, 2003.

Riese, M., Ploeger, F., Rap, A., Vogel, B., Konopka, P., Dameris, M., and Forster, P.: Impact of uncertainties in atmospheric mixing on simulated UTLS composition and related radiative effects, J. Geophys. Res.-Atmos., 117, D16305, https://doi.org/10.1029/2012JD017751, 2012.

Šácha, P., Zajíček, R., Kuchař, A., Eichinger, R., Pišoft, P., and Rieder, H. E.: Disentangling the Advective Brewer-Dobson Circulation Change, Geophys. Res. Lett., 51, e2023GL105919, https://doi.org/10.1029/2023GL105919, 2024.

Santer, B. D.: Behavior of tropopause height and atmospheric temperature in models, reanalyses, and observations: Decadal changes, J. Geophys. Res., 108, 4002, https://doi.org/10.1029/2002JD002258, 2003a.

Santer, B. D.: Contributions of Anthropogenic and Natural Forcing to Recent Tropopause Height Changes, Science, 301, 479–483, https://doi.org/10.1126/science.1084123, 2003b.

Santer, B. D., Wigley, T. M. L., Simmons, A. J., Kållberg, P. W., Kelly, G. A., Uppala, S. M., Ammann, C., Boyle, J. S., Brüggemann, W., Doutriaux, C., Fiorino, M., Mears, C., Meehl, G. A., Sausen, R., Taylor, K. E., Washington, W. M., Wehner, M. F., and Wentz, F. J.: Identification of anthropogenic climate change using a second-generation reanalysis, J. Geophys. Res.-Atmos., 109, D21104, https://doi.org/10.1029/2004JD005075, 2004.

Sausen, R. and Santer, B. D.: Use of changes in tropopause height to detect human influences on climate, Meteorol. Z., 12, 131–136, https://doi.org/10.1127/0941-2948/2003/0012-0131, 2003.

Scherllin-Pirscher, B., Steiner, A. K., Anthes, R. A., Alexander, M. J., Alexander, S. P., Biondi, R., Birner, T., Kim, J., Randel, W. J., Son, S.-W., Tsuda, T., and Zeng, Z.: Tropical Temperature Variability in the UTLS: New Insights from GPS Radio Occultation Observations, J. Climate, 34, 2813–2838, https://doi.org/10.1175/JCLI-D-20-0385.1, 2021.

Schmidt, T., Wickert, J., Beyerle, G., and Heise, S.: Global tropopause height trends estimated from GPS radio occultation data, Geophys. Res. Lett., 35, L11806, https://doi.org/10.1029/2008GL034012, 2008.

Schoeberl, M. R.: Extratropical stratosphere-troposphere mass exchange, J. Geophys. Res.-Atmos., 109, D13303, https://doi.org/10.1029/2004JD004525, 2004.

Seidel, D. J. and Randel, W. J.: Variability and trends in the global tropopause estimated from radiosonde data, J. Geophys. Res., 111, D21101, https://doi.org/10.1029/2006JD007363, 2006.

Seidel, D. J. and Randel, W. J.: Recent widening of the tropical belt: Evidence from tropopause observations, J. Geophys. Res., 112, D20113, https://doi.org/10.1029/2007JD008861, 2007.

Seidel, D. J., Ross, R. J., Angell, J. K., and Reid, G. C.: Climatological characteristics of the tropical tropopause as revealed by radiosondes, J. Geophys. Res.-Atmos., 106, 7857–7878, https://doi.org/10.1029/2000JD900837, 2001.

Simmons, A., Soci, C., Nicolas, J., Bell, B., Berrisford, P., Dragani, R., Flemming, J., Haimberger, L., Healy, S., Hersbach, H., Horányi, A., Inness, A., Munoz-Sabater, J., Radu, R., and Schepers, D.: Global stratospheric temperature bias and other stratospheric aspects of ERA5 and ERA5.1, ECMWF https://doi.org/10.21957/RCXQFMG0, 2020.

Škerlak, B., Sprenger, M., and Wernli, H.: A global climatology of stratosphere–troposphere exchange using the ERA-Interim data set from 1979 to 2011, Atmos. Chem. Phys., 14, 913–937, https://doi.org/10.5194/acp-14-913-2014, 2014.

SPARC: SPARC Reanalysis Intercomparison Project (S-RIP) Final Report, edited by: Fujiwara, M., Manney, G. L., Gray, L. J., and Wright, J. S., SPARC Report No. 10, WCRP-6/2021, https://doi.org/10.17874/800dee57d13, 2022.

Staten, P. W., Lu, J., Grise, K. M., Davis, S. M., and Birner, T.: Re-examining tropical expansion, Nat. Clim. Change, 8, 768–775, https://doi.org/10.1038/s41558-018-0246-2, 2018.

Stohl, A.: Stratosphere-troposphere exchange: A review, and what we have learned from STACCATO, J. Geophys. Res., 108, 8516, https://doi.org/10.1029/2002JD002490, 2003.

Strahan, S. E., Smale, D., Douglass, A. R., Blumenstock, T., Hannigan, J. W., Hase, F., Jones, N. B., Mahieu, E., Notholt, J., Oman, L. D., Ortega, I., Palm, M., Prignon, M., Robinson, J., Schneider, M., Sussmann, R., and Velazco, V. A.: Observed Hemispheric Asymmetry in Stratospheric Transport Trends From 1994 to 2018, Geophys. Res. Lett., 47, e2020GL088567, https://doi.org/10.1029/2020GL088567, 2020.

Tegtmeier, S., Anstey, J., Davis, S., Dragani, R., Harada, Y., Ivanciu, I., Pilch Kedzierski, R., Krüger, K., Legras, B., Long, C., Wang, J. S., Wargan, K., and Wright, J. S.: Temperature and tropopause characteristics from reanalyses data in the tropical tropopause layer, Atmos. Chem. Phys., 20, 753–770, https://doi.org/10.5194/acp-20-753-2020, 2020.

Thomason, L. W., Ernest, N., Millán, L., Rieger, L., Bourassa, A., Vernier, J.-P., Manney, G., Luo, B., Arfeuille, F., and Peter, T.: A global space-based stratospheric aerosol climatology: 1979–2016, Earth Syst. Sci. Data, 10, 469–492, https://doi.org/10.5194/essd-10-469-2018, 2018.

Thompson, D. W. J. and Solomon, S.: Understanding Recent Stratospheric Climate Change, J. Climate, 22, 1934–1943, https://doi.org/10.1175/2008JCLI2482.1, 2009.

Tinney, E. N., Homeyer, C. R., Elizalde, L., Hurst, D. F., Thompson, A. M., Stauffer, R. M., Vömel, H., and Selkirk, H. B.: A Modern Approach to a Stability-Based Definition of the Tropopause, Mon. Weather Rev., 150, 3151–3174, https://doi.org/10.1175/MWR-D-22-0174.1, 2022.

Turhal, K., Plöger, F., Clemens, J., Birner, T., Weyland, F., Konopka, P., and Hoor, P.: Variability and trends in the potential vorticity (PV)-gradient dynamical tropopause, Atmos. Chem. Phys., 24, 13653–13679, https://doi.org/10.5194/acp-24-13653-2024, 2024.

Vallis, G. K., Zurita-Gotor, P., Cairns, C., and Kidston, J.: Response of the large-scale structure of the atmosphere to global warming, Q. J. Roy. Meteor. Soc., 141, 1479–1501, https://doi.org/10.1002/qj.2456, 2015.

Wang, M. and Fu, Q.: Stratosphere-Troposphere Exchange of Air Masses and Ozone Concentrations Based on Reanalyses and Observations, J. Geophys. Res.-Atmos., 126, e2021JD035159, https://doi.org/10.1029/2021JD035159, 2021.

Wang, M., Fu, Q., Solomon, S., Alexander, B., and White, R. H.: Stratosphere-Troposphere Exchanges of Air Mass and Ozone Concentration in the Last Glacial Maximum, J. Geophys. Res.-Atmos., 127, e2021JD036327, https://doi.org/10.1029/2021JD036327, 2022.

Weyland, F.: The mass of the lowermost stratosphere (LMS): LMS mass calculation and trends in five reanalyses for the time period 1979–2019, Zenodo [data set], https://doi.org/10.5281/zenodo.13890232, 2024.

Wilcox, L. J., Hoskins, B. J., and Shine, K. P.: A global blended tropopause based on ERA data. Part II: Trends and tropical broadening, Q. J. Roy. Meteor. Soc., 138, 576–584, https://doi.org/10.1002/qj.910, 2012.

World Meteorological Organization (WMO): Definition of the tropopause, WMO Bulletin, 6, 136–138, 1957.

World Meteorological Organization (WMO): Scientific assessment of ozone depletion, 2002, World Meteorological Organisation Global Ozone Research and Monitoring Project – Report No.47, Geneva, Switzerland, 498 pp., https://csl.noaa.gov/assessments/ozone/2002/ (last access: 20 January 2025), 2003.

Xian, T. and Homeyer, C. R.: Global tropopause altitudes in radiosondes and reanalyses, Atmos. Chem. Phys., 19, 5661–5678, https://doi.org/10.5194/acp-19-5661-2019, 2019.

Zambri, B., Solomon, S., Thompson, D. W. J., and Fu, Q.: Emergence of Southern Hemisphere stratospheric circulation changes in response to ozone recovery, Nat. Geosci., 14, 638–644, https://doi.org/10.1038/s41561-021-00803-3, 2021.

Zhang, Y., Rossow, W. B., Lacis, A. A., Oinas, V., and Mishchenko, M. I.: Calculation of radiative fluxes from the surface to top of atmosphere based on ISCCP and other global data sets: Refinements of the radiative transfer model and the input data, J. Geophys. Res.-Atmos., 109, 2003JD004457, https://doi.org/10.1029/2003JD004457, 2004.

Zou, L., Hoffmann, L., Müller, R., and Spang, R.: Variability and trends of the tropical tropopause derived from a 1980–2021 multi-reanalysis assessment, Front. Earth Sci., 11, 1177502, https://doi.org/10.3389/feart.2023.1177502, 2023.

Zängl, G. and Hoinka, K. P.: The Tropopause in the Polar Regions, J. Climate, 14, 3117–3139, https://doi.org/10.1175/1520-0442(2001)014<3117:TTITPR>2.0.CO;2, 2001.